Cellular & Molecular Immunology www.nature.com/cmi

ARTICLE

NLRP3-dependent pyroptosis is required for HIV-1 gp120-induced neuropathology

Xiaolong He[1], Weijun Yang[1], Zhijie Zeng[1], Yi Wei[1], Jie Gao[1], Bao Zhang[1], Li Li[2], Liqun Liu[3], Yu Wan[1], Qing Zeng[1], Zelong Gong[1], Liting Liu[4], Hanyun Zhang[1], Yubin Li[1], Shaojie Yang[1], Tongtong Hu[1], Lixian Wu[4], Eliezer Masliah[5,6], Shenghe Huang[1,2,7] and Hong Cao[1]

The human immunodeficiency virus-1 (HIV-1) envelope protein gp120 is the major contributor to the pathogenesis of HIV-associated neurocognitive disorder (HAND). Neuroinflammation plays a pivotal role in gp120-induced neuropathology, but how gp120 triggers neuroinflammatory processes and subsequent neuronal death remains unknown. Here, we provide evidence that NLRP3 is required for gp120-induced neuroinflammation and neuropathy. Our results showed that gp120-induced NLRP3-dependent pyroptosis and IL-1β production in microglia. Inhibition of microglial NLRP3 inflammasome activation alleviated gp120-mediated neuroinflammatory factor release and neuronal injury. Importantly, we showed that chronic administration of MCC950, a novel selective NLRP3 inhibitor, to gp120 transgenic mice not only attenuated neuroinflammation and neuronal death but also promoted neuronal regeneration and restored the impaired neurocognitive function. In conclusion, our data revealed that the NLRP3 inflammasome is important for gp120-induced neuroinflammation and neuropathology and suggest that NLRP3 is a potential novel target for the treatment of HAND.

Keywords: NLRP3 inflammasome; HIV-1 gp120; HIV-associated neurocognitive disorder; Neuroinflammation; Neuropathology

Cellular & Molecular Immunology (2020) 17:283–299; https://doi.org/10.1038/s41423-019-0260-y

INTRODUCTION

Human immunodeficiency virus-1 (HIV-1) infection not only impairs immune function but also causes neuronal death, resulting in HIV-associated neurocognitive disorders (HAND).[1,2] Although antiretroviral therapy (ART) effectively decreases the HIV burden in the central nervous system (CNS), mild and moderate forms of HAND remain prevalent and affect the quality of life.[3] This phenomenon indicates that ART fails to provide effective protection against HIV-associated neurotoxicity and that effective neuroprotective agents are needed. HAND is a complicated neurodegenerative disease characterized by widespread, progressive neuronal death and dementia. The HIV-1 envelope protein gp120 is believed to be involved in the pathogenesis of HAND.[4–7] This view is strongly supported by the finding that gp120 transgenic (Tg) mice display typical neuropathological and behavioral deficits characteristic of HAND.[5,8] Further studies have provided convincing evidence that the chronic neuroinflammatory response is the major pathogenic player in gp120-induced neuropathology.[6,9,10] However, how gp120 triggers neuroinflammation and neuronal death is largely unknown.

Inflammasomes are multiprotein complexes that are often composed of Nod-like receptors (NLR), apoptosis-associated speck-like proteins containing a caspase recruitment domain (ASC) and caspase-1 precursor (pro-caspase-1).[11] The NLRP3 inflammasome is the best-characterized inflammasome,[12] which recognizes a range of stimuli via NLR, forming a complex (ASC speck) to activate caspase-1. Activated caspase-1 then cleaves the pore-forming protein gasdermin D (GSDMD), interleukin-1β precursor (pro-IL-1β) and interleukin-18 precursor (pro-IL-18), resulting in pyroptosis, IL-1β, and IL-18 release.[12] Pyroptosis is a type of proinflammatory programmed cell death mediated by caspase-1-cleaved GSDMD (N-terminal fragment, GSDMD-N),[13] which binds to the membrane to form membrane pores and promote the release of proinflammatory mediators, notably, IL-1β. This cytokine plays a pivotal role in the initiation and continuation of neuroinflammation and neuropathology[14] because most neuronal cells express the IL-1 receptor, making the CNS particularly sensitive to IL-1β.[15] In the context of common neurodegenerative disorders, such as Alzheimer's disease and Parkinson's disease, persistent stimulation of misfolded proteins (amyloid-β or α-synuclein) triggers chronic NLRP3 inflammasome activation, resulting in neuroinflammation and neuropathology.[16,17] Interestingly, caspase-1, IL-1β, and IL-18 were induced in the brains of HIV-infected individuals in an analysis of

[1]Department of Microbiology, Guangdong Provincial Key Laboratory of Tropical Disease Research, School of Public Health, Southern Medical University, Guangzhou 510515, China; [2]Kunming Key Laboratory of Children Infection and Immunity, Yunnan Institute of Pediatrics, Kunming Children's Hospital, Kunming, Yunnan 650228, China; [3]Department of Pediatrics, The Second Xiangya Hospital, Central South University, Changsha 410011, China; [4]Department of Medical Microbiology and Immunology, Dali University, Dali 671000, China; [5]Division of Neurosciences, National Institute on Aging, National Institutes of Health, Bethesda, MD 20892, USA; [6]Departments of Neuroscience and Pathology, University of California, San Diego, La Jolla, CA 92093, USA and [7]Saban Research Institute, Children's Hospital Los Angeles, University of Southern California, Los Angeles, CA 90027, USA

Correspondence: Shenghe Huang (shhuang@usc.edu) or Hong Cao (gzhcao@smu.edu.cn)

These authors contributed equally: Xiaolong He, Weijun Yang, Zhijie Zeng, Yi Wei

Received: 11 December 2018 Accepted: 21 June 2019
Published online: 18 July 2019

inflammasome-associated genes.[18] However, whether NLRP3-dependent pyroptosis is involved in gp120-induced neuropathology remains unclear.

The purpose of this study was to explore whether the NLRP3 inflammasome plays a role in gp120-induced neuropathology. We have mainly focused on the neurotoxic mechanism of gp120 LAV from CXCR4-preferring HIV-1 isolates because these isolates often determine progression to AIDS- and HIV-1-associated dementia.[19–21] We found that gp120 LAV triggered NLRP3-dependent pyroptosis and IL-1β release in microglia. Inhibition of NLRP3 suppressed gp120 LAV-mediated neurotoxic factor release and neuronal injury. Moreover, we demonstrated that treatment of gp120 LAV Tg mice with MCC950, a small-molecule inhibitor of NLRP3, led to a significant restoration of neuronal integrity and neurocognitive function. Conclusively, our data revealed that NLRP3 is essential for gp120-induced neuropathology.

RESULTS

HIV-1 gp120 LAV induces microglial inflammasome activation in vitro and in vivo

Generally, inflammasome activation requires two stages.[22] The first stage is priming, in which inflammasome components are transcribed and expressed. This stage is followed by the processing stage, in which the inflammasome components are assembled (namely, ASC speck), leading to caspase-1 activation, GSDMD cleavage, pyroptosis, and bioactive IL-1β release. We first found that gp120 LAV caused the formation of ASC oligomers in a mouse microglial line (BV2) (Fig. 1a). Using fluorescence microscopy, we demonstrated that gp120 LAV induced the formation of a single bright spot of green fluorescence (ASC specks) in the cytoplasm (Fig. 1b, c), indicating that gp120 LAV caused the assembly of inflammasome components. Interestingly, a proportion of ASC specks were observed outside of the cells (Supplementary Fig. 1a, red arrows and 1b), concurring with the findings that were recently documented in HIV-1-infected patients.[23,24] Notably, we found that gp120 LAV induced ASC specks without lipopolysaccharide (LPS) priming, while adenosine triphosphate (ATP), a known inflammasome-activating agent, did not significantly induce ASC specks under the same conditions, indicating that gp120 LAV might participate in both the priming and processing stages of inflammasome activation.

Next, we detected the critical events of inflammasome activation, including caspase-1 cleavage, pyroptosis and IL-1β maturation. As shown in Fig. 1d, e, stimulation with gp120 LAV induced a significant increase in caspase-1 activity and IL-1β release, whereas these effects were not shown in the control group and the group with ATP stimulation alone. Then, we performed Western blotting to confirm whether caspase-1 and IL-1β are released as their mature forms. As expected, activated caspase-1 (Casp-1-p20) and IL-1β (IL-1β-p17) were observed in the culture supernatants of BV2 upon gp120 LAV stimulation (Fig. 1f). Furthermore, we found that gp120 LAV stimulation cleaved GSDMD to produce GSDMD-N (Fig. 1g, upper panel) and enhanced lactate dehydrogenase (LDH) release (Fig. 1g, lower panel), and these actions were significantly suppressed by the caspase-1 inhibitor Z-YVAD-fmk, indicating that gp120 LAV-induced LDH release was mediated by pyroptosis but not necrosis. More importantly, these critical events of inflammasome activation were also observed in gp120 LAV-treated primary mouse microglia (Supplementary Fig. 2a-c). Together, these data suggested that gp120 LAV induced a significant activation of the inflammasome in microglia.

To confirm the above findings in vivo, we further measured the critical events of inflammasome activation in the brain tissue of gp120 LAV Tg mice, which express soluble gp120 LAV in astrocytes using the glial fibrillary acidic protein (GFAP) promoter.[5] The results showed that gp120 LAV Tg mice had higher caspase-1 activity and IL-1β levels than wild type (WT) mice (Fig. 1h, i). Western blot assays showed that active caspase-1 and mature IL-1β were also more highly expressed in the brain tissue homogenates of gp120 LAV Tg mice than in the WT mice, and treatment with the caspase-1-specific inhibitor Z-YVAD-fmk reduced these events (Fig. 1j, k). Furthermore, immunohistochemical staining of GSDMD showed that pyroptosis was more obvious in the hippocampal sections of gp120 LAV Tg mice than in the WT mice (Fig. 1l). The results of in situ immunofluorescence staining showed that activated caspase-1 and GSDMD were colocalized with the microglial marker Iba-1 (ionized calcium binding adapter molecule 1) in the brains of gp120 LAV Tg mice (Supplementary Fig. 3a, b). Collectively, these data demonstrated that gp120 LAV can stimulate microglial inflammasome activation.

NLRP3 is essential for gp120 LAV-mediated inflammasome activation

Because NLRP1, NLRP3, absent in melanoma-2 (AIM2) and NLR family CARD-containing protein 4 (NLRC4) are highly expressed in microglia,[11] we selected them to determine which sensor is involved in gp120 LAV-induced inflammasome activation. As shown in Fig. 2a–c, knockdown of NLRP1, AIM2 or NLRC4 had no inhibitory effect on gp120 LAV-induced caspase-1 activation, GSDMD cleavage, and LDH and IL-1β release, whereas these events were obviously decreased when NLRP3 expression was reduced. Notably, higher IL-1β release was still detected in the gp120 LAV-treated si-*NLRP3* group compared to the control group, indicating that gp120 LAV-induced IL-1β release may also be mediated in a non-caspase-1-dependent manner. Furthermore, we found that knockdown of ASC or caspase-1 significantly alleviated caspase-1 activation, GSDMD cleavage, and LDH and IL-1β release (Fig. 2d–f), suggesting that gp120 LAV-induced inflammasome activation is controlled by the NLRP3-ASC-caspase-1 pathway. To further investigate this issue, we used a specific inhibitor of the NLRP3 inflammasome, MCC950,[25] to confirm the findings mentioned above and support the possibility of using MCC950 for the treatment of gp120 LAV-induced neuropathology. As expected, MCC950 significantly decreased gp120 LAV-induced pyroptosis and IL-1β release (Fig. 2g, h). More importantly, MCC950-mediated inhibition of inflammasome activation was also observed in gp120-treated primary mouse microglia (Supplementary Fig. 2d–f). Together, these results indicated that NLRP3 was required for gp120 LAV-induced inflammasome activation.

Because LPS priming is dispensable for gp120 LAV-induced inflammasome activation (Fig. 1a–g), we then investigated whether gp120 LAV is involved in the priming stage of NLRP3 inflammasome activation. Western blot analysis showed that gp120 LAV induced IκBα degradation and NF-κB p65 nuclear translocation and enhanced the expression of NLRP3 and pro-IL-1β (Fig. 2i–m, Supplementary Fig. 2g-k), demonstrating that gp120 LAV participates in the priming stage of NLRP3 inflammasome activation. Based on the above results (Figs. 1 and 2, Supplementary Figs. 1–3), we concluded that gp120 LAV could induce microglial NLRP3 inflammasome activation.

The CXCR4-Kv1.3 pathway is necessary for gp120 LAV-induced NLRP3 inflammasome activation

K^+ efflux, reactive oxygen species (ROS) production, phagocytosis and lysosomal injury are the common cellular mechanisms responsible for regulating NLRP3 inflammasome activation.[26] Thus, we next investigated whether these events were implicated in gp120 LAV-induced IL-1β release. Using enzyme-linked immunosorbent assays (ELISAs), we demonstrated that gp120 LAV-induced IL-1β production was reduced in a dose-dependent manner when K^+ efflux was suppressed by the addition of a high concentration of K^+ or glyburide (K^+ efflux inhibitor) (Fig. 3a). Pretreatment of BV2 cells with the ROS inhibitors N-acetyl-L-

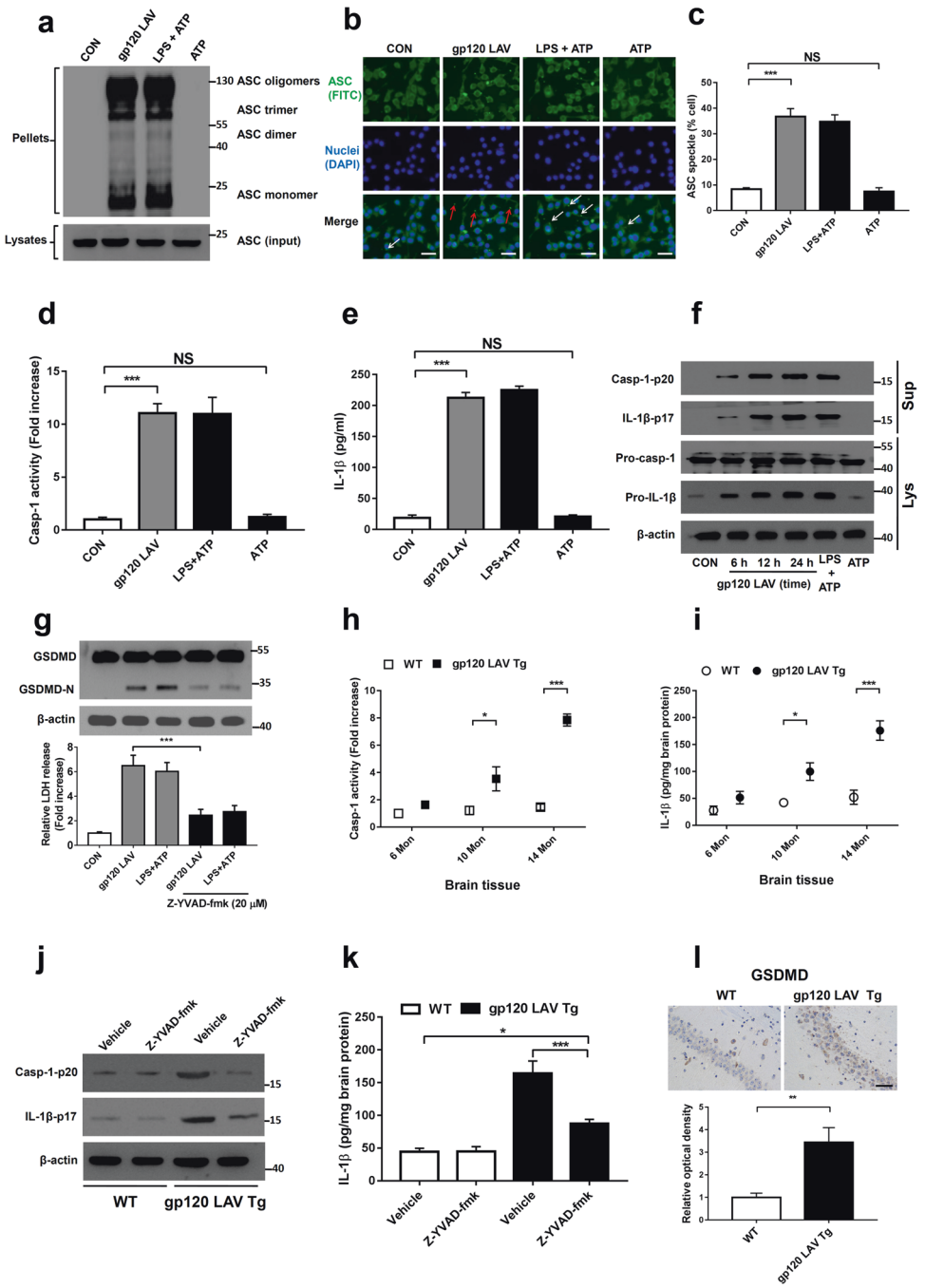

Fig. 1 HIV-1 gp120 LAV induces inflammasome activation in vitro and in vivo. **a**–**c** Western blot of ASC in crosslinked pellets (upper panel) and cell lysates (lower panel) (**a**) and fluorescence microscopy of ASC specks (**b**) of BV2 cells treated with control, gp120 LAV (0.5 μg/ml), LPS + ATP or ATP. The arrows indicate speck formation, scale bar: 20 μm. **c** The percentages of ASC specks in BV2 cells. Cells primed with LPS and stimulated with ATP (LPS + ATP) served as a positive control. **d**, **e** Caspase-1 activity (**d**) and IL-1β release (**e**) in supernatants from BV2 cells treated with control, gp120 LAV (0.5 μg/ml), LPS + ATP or ATP. The data in (**d**) are expressed as the ratio of the absorbance determined from the treated cells to that of the control. **f** Western blots of activated caspase-1 (Casp-1-p20) and cleaved IL-1β (IL-1β-p17) in culture supernatants (Sup) from BV2 cells treated with gp120 LAV (0.5 μg/ml) at different times. Pro-casp-1 and pro-IL-1β in cell lysates (Lys) were also detected. **g** GSDMD immunoblot analysis (upper panel) and LDH release (lower panel) of BV2 cells treated with gp120 LAV (0.5 μg/ml) in the absence or presence of Z-YVAD-fmk (20 μM). LDH data are expressed as the ratio of the absorbance determined from the treated cells to that of the control. **h**, **i** Caspase-1 activity (**h**) and IL-1β level (**i**) in brain tissues of WT and gp120 LAV transgenic (Tg) mice at different ages (6, 10, 14 months, Mon, $n = 5$). **j**, **k** WT ($n = 5$) and gp120 LAV Tg mice ($n = 5$) treated with or without Z-YVAD-fmk (10 mg/kg body weight) for 30 days. Then, all mice were euthanized by CO_2 inhalation, and the brain tissue was harvested and homogenized. **j** Immunoblots of Casp-1-p20 and IL-1β-p17 and **k** ELISA of IL-1β in brain tissue homogenates. **l** Representative images of immunolabeled GSDMD from the hippocampal section of WT and gp120 LAV Tg mice ($n = 3$, upper panel); optical density was analyzed quantitatively ($n = 6$, lower panel), Scale bar: 50 μm. The data are displayed as the mean ± SEM ($n = 5$, **c**, **d**, **e**, **g**, **h**, **i**, **k**; $n = 6$, **l**) from three independent experiments. The western blot, fluorescence and immunohistochemical results are representative of three independent experiments (**a**, **b**, **f**, **g**, **j**, **l**). *$P < 0.05$, **$P < 0.01$, ***$P < 0.001$; NS, no significance

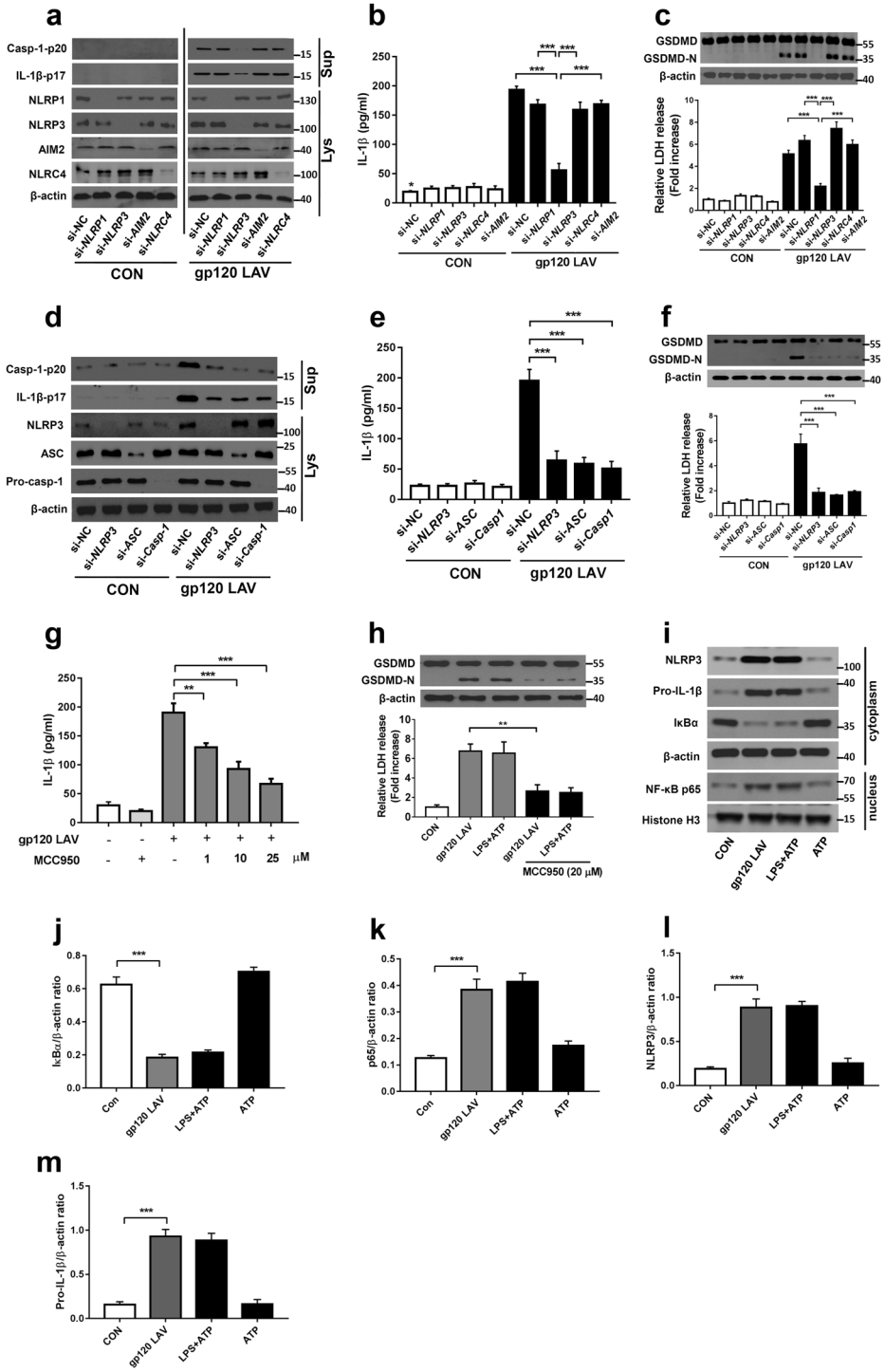

Fig. 2 NLRP3 is critical for gp120 LAV-induced inflammasome activation. **a**–c Western blots of Casp-1-p20 and IL-1β-p17 (**a**) and the levels of IL-1β (**b**) and LDH (**c**, lower panel) in supernatants (Sup) from BV2 cells transfected with control siRNA (si-NC) or *NLRP1*, *NLRP3*, *AIM2*, and *NLRC4*-specific siRNA and stimulated for 24 h with or without gp120 LAV (0.5 μg/ml). The NLRP1, NLRP3, AIM2, NLRC4 (**a**) and GSDMD (**c**, upper panel) in lysates (Lys) of those cells were detected. **d–f** Western blots of Casp-1-p20 and IL-1β-p17 (**d**) and the levels of IL-1β (**e**) and LDH (**f**, lower panel) in supernatants from BV2 cells transfected with control siRNA or *NLRP3*, *ASC*, and *Casp-1*-specific siRNA and stimulated with or without gp120 LAV (0.5 μg/ml). The NLRP3, ASC, pro-casp-1 (**d**) and GSDMD (**f**, upper panel) in lysates of those cells were detected. **g** ELISA of IL-1β in supernatants of BV2 cells treated with gp120 LAV (0.5 μg/ml) in the presence of various doses of the NLRP3-specific inhibitor (MCC950, 1–25 μM). **h** GSDMD immunoblot analysis (upper panel) and relative LDH release (lower panel) of BV2 cells treated with gp120 LAV (0.5 μg/ml) in the absence or presence of MCC950 (20 μM). **i–k** Western blots (**i**) and densitometric analysis of IκBα (**j**), NF-κB p65 (**k**), NLRP3 (**l**), and pro-IL-1β (**m**) in BV2 cells treated with the control, gp120 LAV (0.5 μg/ml), LPS + ATP or ATP. The data are displayed as the mean ± SEM ($n = 5$) from three independent experiments (**b**, **c**, **e**–**h**, **j**–**m**). Western blot results are representative of three (**a**, **c**, **d**, **f**, **h**) and five (**i**) independent experiments. $^{**}P < 0.01$, $^{***}P < 0.001$; NS, no significance

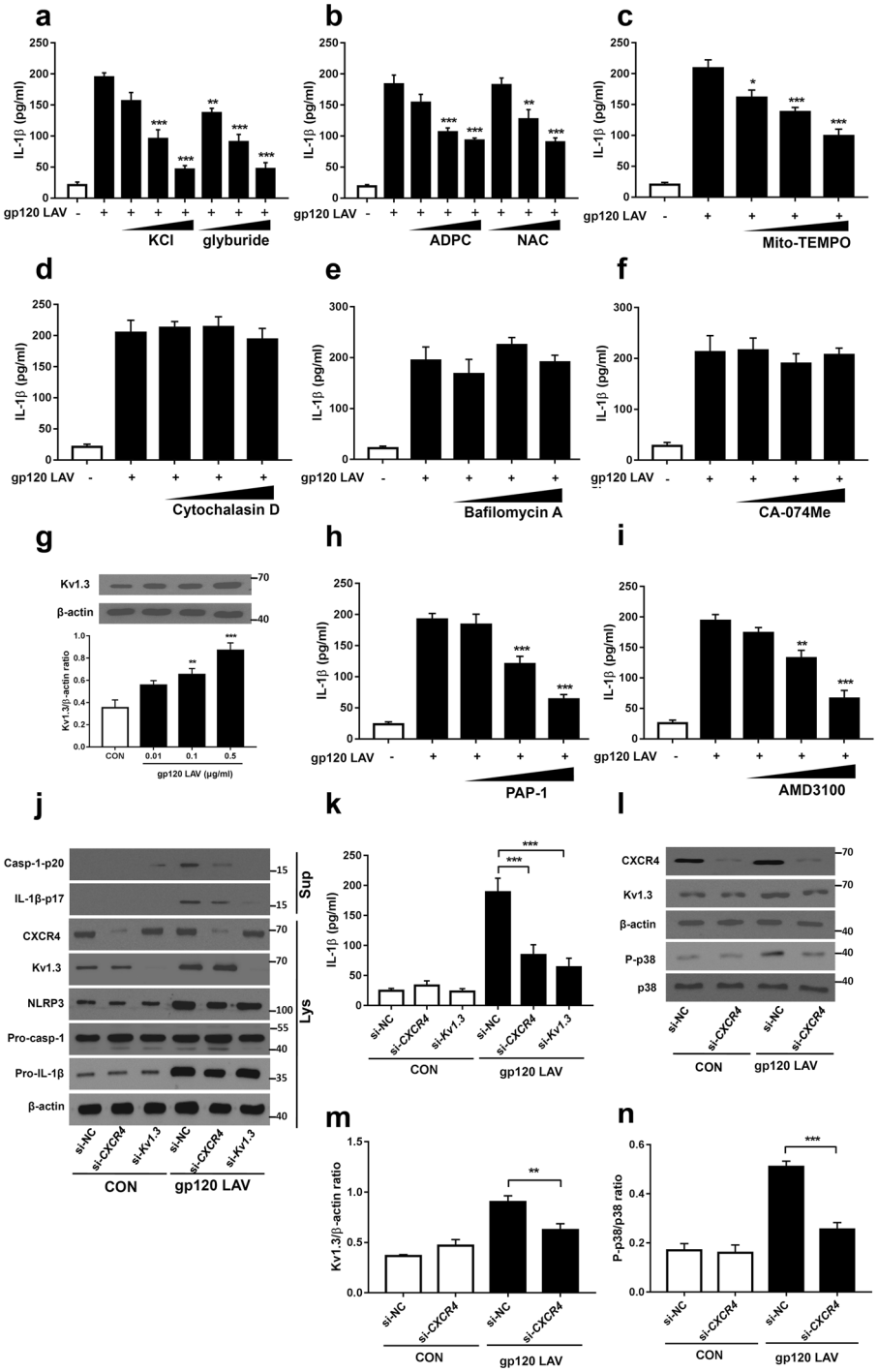

Fig. 3 The CXCR4-Kv1.3 axis is implicated in gp120 LAV-induced NLRP3 inflammasome activation. **a–f** ELISA of IL-1β in supernatants of BV2 cells stimulated by gp120 LAV (0.5 μg/ml) in the presence of increasing doses of KCl (50–200 mM), the K^+ efflux inhibitor glyburide (50–200 μM) (**a**); the ROS inhibitor ADPC (5–50 μM), NAC (5–25 μM) (**b**); MitoTEMPO (100–500 μM) (**c**); the actin polymerization inhibitor cytochalasin D (1–25 μM) (**d**); the lysosome inhibitor bafilomycin A (10–200 nM) (**e**); and the cathepsin B inhibitor CA-074Me (5–20 μM) (**f**). **g** Western blot (upper panel) and densitometric analysis (lower panel) of Kv1.3 in lysates of BV2 cells stimulated with increasing doses of gp120 LAV (0.01–0.5 μg/ml). **h**, **i** ELISA of IL-1β in supernatants of BV2 cells stimulated with gp120 LAV (0.5 μg/ml) in the presence of increasing doses of a Kv1.3-specific inhibitor (PAP-1, 0.1–2 μM) (**h**) or CXCR4-specific inhibitor (AMD3100, 0.1–10 μM) (**i**). **j**, **k** Immunoblot analysis of Casp-1-p20 and IL-1β-p17 (**j**) and ELISA of IL-1β (**k**) in supernatants (Sup) of BV2 cells transfected with control siRNA, *CXCR4* or *Kv1.3*-specific siRNA and treated with or without gp120 LAV (0.5 μg/ml). CXCR4, Kv1.3, NLRP3, pro-casp-1, and pro-IL-1β in lysates (Lys) of these cells were also detected. **l**–**n** Western blots (**l**) and densitometric analysis of Kv1.3 (**m**) and p38-MAPK phosphorylation (P-p38, **n**) in lysates of BV2 cells transfected with siRNA control or *CXCR4*-specific siRNA and stimulated with or without gp120 LAV (0.5 μg/ml). The data are displayed as the mean ± SEM ($n = 5$) from three independent experiments (**a**–**i**, **k**, **m**, **n**). The Western blot results are representative of three (**j**) and five (**g**, **l**) independent experiments. $^*P < 0.05$, $^{**}P < 0.01$, $^{***}P < 0.001$

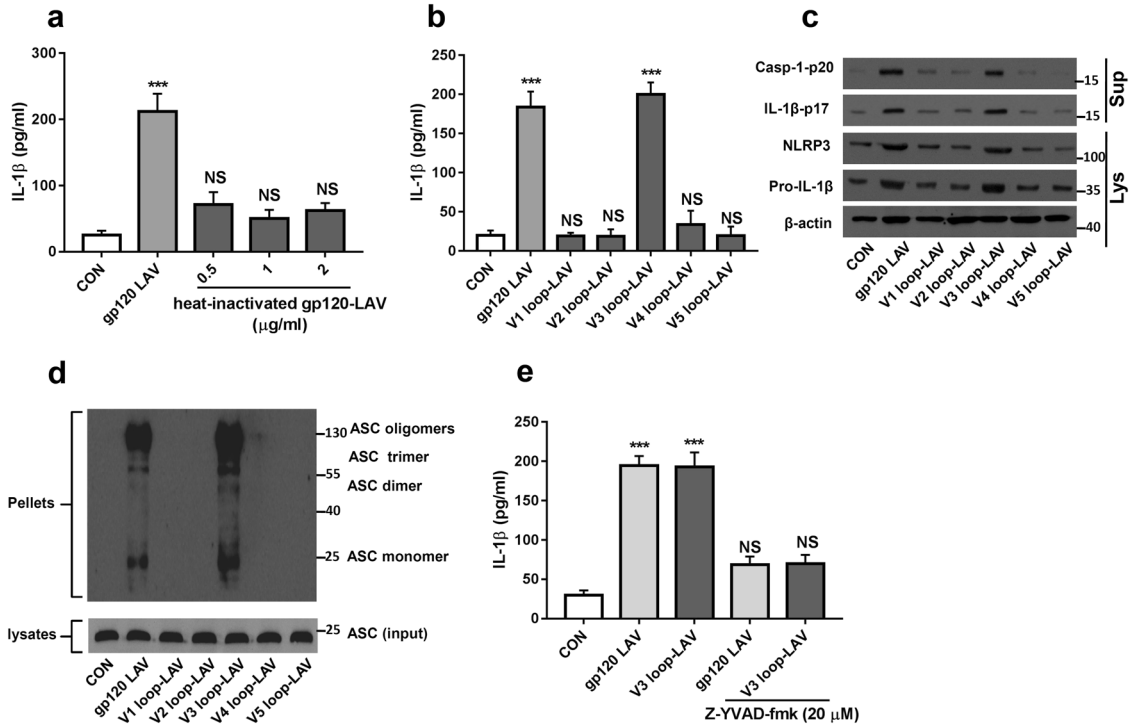

Fig. 4 The V3 loop is involved in gp120 LAV-induced NLRP3 inflammasome activation. **a** Production of IL-1β from BV2 cells stimulated with gp120 LAV (0.5 μg/ml) or increasing doses of heat-inactivated gp120 LAV (0.5–2 μg/ml) for 24 h. **b**, **c** ELISA of IL-1β (**b**) and western blots of Casp-1-p20 and IL-1β-p17 (**c**) in supernatants of BV2 cells stimulated with gp120 LAV (0.5 μg/ml) or the different variable loop peptides (V1–V5 loops, 0.2 μg/ml) for 24 h. NLRP3, pro-caspase-1, and pro-IL-1β in cell lysates (Lys) were also detected. **d** Immunoblot analysis of ASC in crosslinked pellets (upper panel) and cell lysates (lower panel) of BV2 cells stimulated with gp120 LAV (0.5 μg/ml) or the different variable loop peptides (V1–V5 loops, 0.2 μg/ml) for 24 h. **e** IL-1β in supernatants of BV2 cells treated with gp120 LAV (0.5 μg/ml) or V3 loop peptide (0.2 μg/ml) in the absence or presence of Z-YVAD-fmk (20 μM). The data are displayed as the mean ± SEM ($n = 5$) from three independent experiments (**a**, **b**, **e**). Western blot results are representative of two (**d**) and three (**c**) independent experiments. ***$P < 0.001$; NS, no significance

cysteine (NAC), (2R, 4R)-4-aminopyrrolidine-2,4-dicarboxylate (APDC) or MitoTEMPO also dose-dependently suppressed gp120 LAV-induced IL-1β release (Fig. 3b, c). These results indicated that both K^+ efflux and ROS generation are essential for gp120 LAV-induced inflammasome activation. In contrast, both the actin polymerization inhibitor cytochalasin D, the lysosome inhibitor bafilomycin A and the cathepsin B inhibitor Ca-074Me had no significant effect on gp120 LAV-induced IL-1β release (Fig. 3d–f). Importantly, cytotoxic assays showed that all the concentrations of inhibitors used here did not induce significant cytotoxicity (Supplementary Fig. 4a-h), suggesting that the decreased IL-1β release was not due to cell death. Together, these findings implied that K^+ efflux and ROS production, but not phagocytosis, are important for gp120 LAV-induced IL-1β production.

Recent studies have reported that Kv1.3 is required for gp120 LAV-mediated K^+ efflux and neuronal death.[27,28] However, whether Kv1.3 is necessary for gp120 LAV-induced NLRP3 inflammasome activation is unclear. We first assessed the expression of Kv1.3 in microglia upon gp120 LAV stimulation. Western blotting showed that gp120 LAV enhanced the expression of Kv1.3 in a dose-dependent manner (Fig. 3g). Then, we used the Kv1.3 inhibitor PAP-1 and Kv1.3-specific siRNA to explore the role of Kv1.3 in gp120 LAV-induced inflammasome activation. ELISA and western blotting results showed that both genetic disruption and pharmacological blockade of Kv1.3 resulted in a marked reduction in caspase-1 activation and IL-1β release (Fig. 3h, j, k), indicating that Kv1.3 is involved in gp120 LAV-induced inflammasome activation. Previous studies demonstrated that gp120 LAV induced K^+ efflux via the chemokine receptor CXCR4 and p38-mitogen-activated protein kinase (MAPK) signaling;[27,28] we thus directly examined whether CXCR4 is required for gp120 LAV-induced NLRP3 inflammasome activation. As expected, both genetic inactivation and pharmacological blockade of CXCR4 (using the CXCR4-specific inhibitor AMD3100) resulted in a strong reduction in caspase-1 activation and IL-1β release (Fig. 3i–k). CXCR4 knockdown also significantly reduced gp120 LAV-induced Kv1.3 expression and p38-MAPK phosphorylation (Fig. 3l–n). Collectively, these results indicated that CXCR4-Kv1.3 signaling was needed for gp120 LAV-induced NLRP3 inflammasome activation.

We then sought to map the region(s) of gp120 LAV that are involved in NLRP3 inflammasome activation. First, we noted that heat-treated gp120 LAV has no effect on IL-1β production (Fig. 4a), suggesting that a native gp120 LAV protein is necessary for processing of pro-IL-1β. Because the third variable loop (V3 loop) is important for gp120 LAV-mediated proinflammatory responses and neuronal death,[29] we next investigated whether this region is implicated in NLRP3 inflammasome activation. BV2 cells were treated with V1, V2, V3, V4, or V5 loops. ELISA results showed that only the V3 loop caused a significant increase in IL-1β release (Fig. 4b). We further found that the V3 loop enhanced NLRP3 and pro-IL-1β expression and induced ASC speck formation, caspase-1 activation and IL-1β maturation (Fig. 4c, d). The inhibition of caspase-1 activation significantly reduced V3 loop-induced IL-1β release (Fig. 4e). These data indicated that the V3 loop of gp120 LAV is implicated in NLRP3 inflammasome activation.

The NLRP3-IL-1β axis is critical for gp120 LAV-induced release of neurotoxic factors and neuronal injury in vitro

IL-1β signaling plays a key role in the initiation and continuation of neuroinflammation.[15] A previous study demonstrated that gp120 LAV-induced IL-1β contributed to the production of neurotoxic

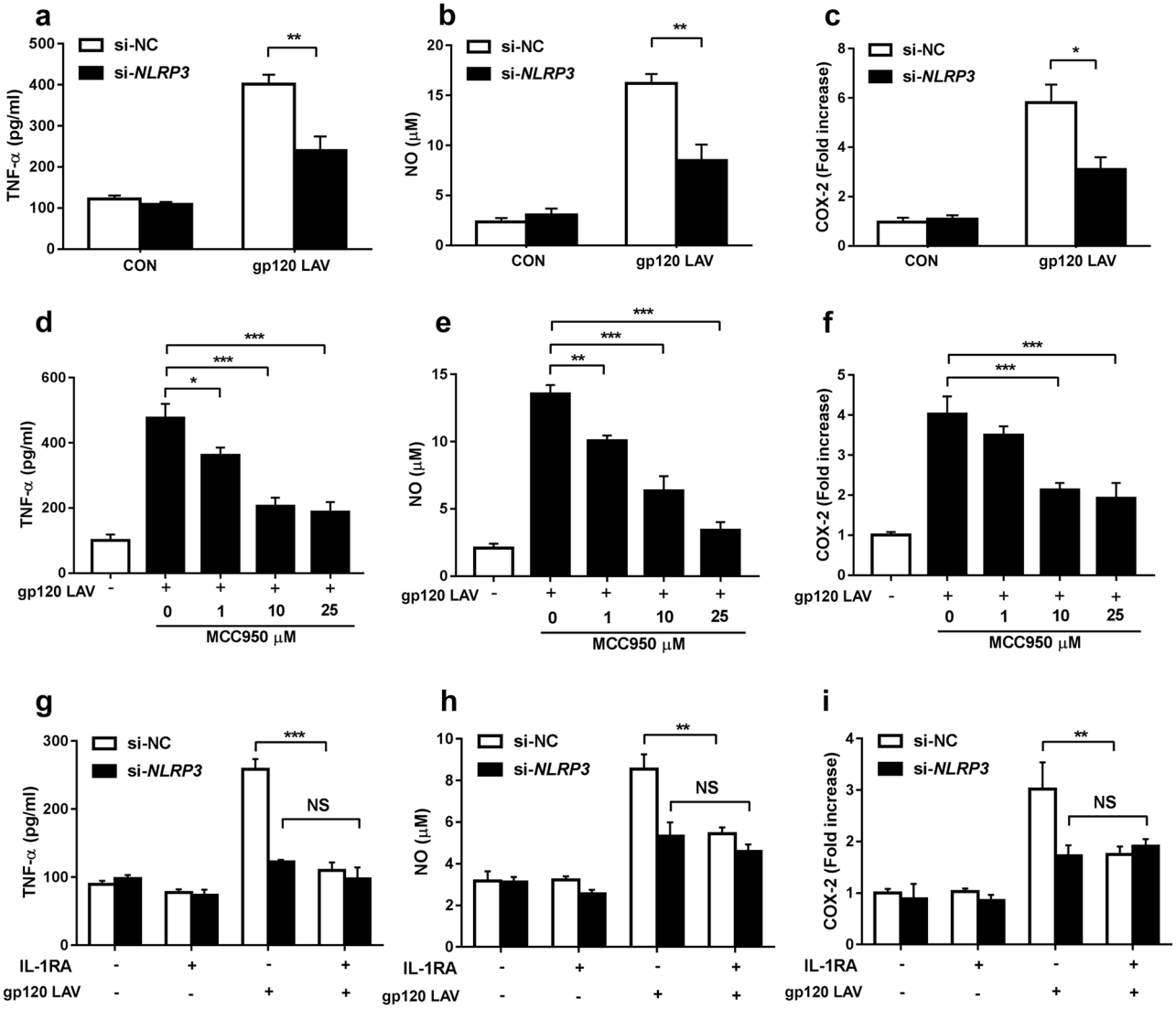

Fig. 5 HIV-1 gp120 LAV-induced neurotoxic mediator release is mediated by the NLRP3-IL-1β-axis. **a**–**c** Production of TNF-α (**a**), NO (**b**), and COX-2 (**c**) by BV2 cells transfected with control siRNA or *NLRP3*-specific siRNA and stimulated with or without gp120 LAV (0.5 μg/ml). **d**–**f** Production of TNF-α (**d**), NO (**e**), and COX-2 (**f**) by BV2 cells stimulated with gp120 LAV (0.5 μg/ml) in the presence of various doses of the NLRP3-specific inhibitor MCC950 (1–25 μM). **g**–**i** Production of TNF-α (**g**), NO (**h**), and COX-2 (**i**) by normal BV2 cells treated with culture supernatants from gp120 LAV-treated si-NC or si-*NLRP3* BV2 cells in the absence or presence of IL-1RA (1 μg/ml). The data are displayed as the mean ± SEM ($n = 5$) from three independent experiments (**a**–**i**). $^{*}P < 0.05$, $^{**}P < 0.01$, $^{***}P < 0.001$; NS, no significance

mediators, including tumor necrosis factor-α (TNF-α), nitric oxide (NO), and cyclooxygenase-2 (COX-2).[30] We next investigated whether blockade of NLRP3 could decrease gp120 LAV-induced secretion of these neurotoxic factors. As shown in Fig. 5a–f, both genetic disruption and pharmacological blockade of NLRP3 considerably suppressed gp120 LAV-induced production of TNF-α, NO, and COX-2. Furthermore, MCC950-mediated inhibition of neurotoxic factor release was observed in gp120 LAV-treated mouse primary microglial cells (Supplementary Fig. 5a-c).

The IL-1 receptor antagonist IL-1RA was used to ensure that the downstream effector of NLRP3 is IL-1β. We collected culture supernatants from gp120 LAV-treated si-negative control (si-NC) or si-*NLRP3* BV2 cells, and these supernatants were used to treat normal BV2 cells in the presence or absence of IL-1RA pretreatment. Our results showed that the supernatants from gp120 LAV-treated si-NC BV2 cells induced TNF-α, NO, and COX-2 production, but their levels were considerably reduced by IL-1RA pretreatment (Fig. 5g–i), indicating that the production of TNF-α, NO, and COX-2 depends on autocrine and/or paracrine effects of IL-1β. Notably, NLRP3 knockdown abolished the effect of IL-1RA-mediated reduction of these neurotoxic mediators (Fig. 5g–i), suggesting that gp120 LAV-induced production of these neurotoxic mediators specifically depended on the NLRP3-IL-1β axis.

We further investigated whether NLRP3 contributes to gp120 LAV-induced neuronal injury in vitro. Immunofluorescence analysis showed that the culture supernatants from gp120 LAV-stimulated microglial cells induced obvious dendritic injury, as reflected by a significantly reduced neurite length (immunostained with the microtubule-associated protein 2, MAP-2) when compared with the control (Supplementary Fig. 5d, e). The neurotoxic effect of the culture supernatant was blocked when microglial NLRP3 was inhibited by MCC950 (Supplementary Fig. 5d, e). To exclude the potential carry-over effect of MCC950 on neurons, we set a control group, in which MCC950 was added to the culture supernatants of gp120 LAV-stimulated microglial cells before treatment of the neurons [indicated as MCC950 (be.) in Supplementary Fig. 5d, e]. MCC950 (be.) seemingly exerted a slight protective effect on neurons, which was not significant, indicating

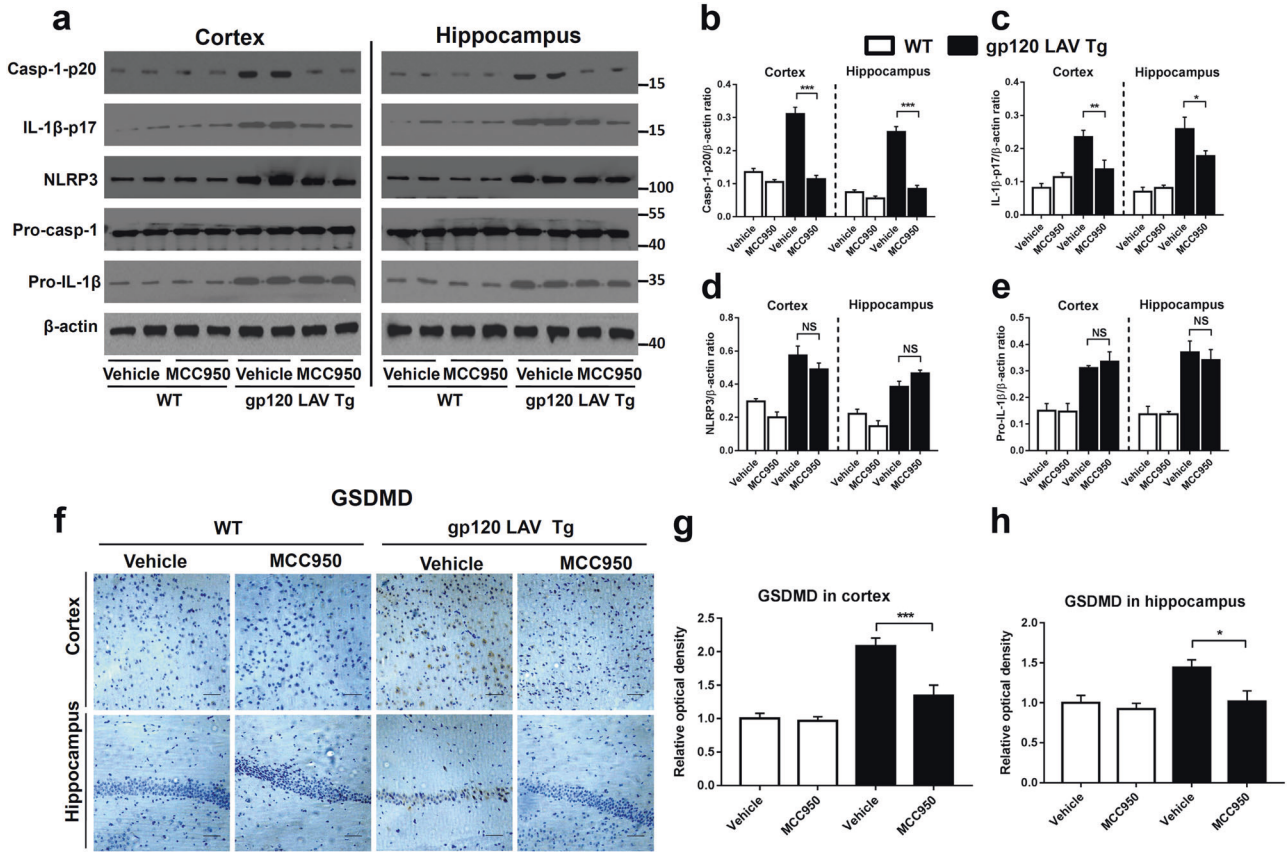

Fig. 6 Effect of MCC950 on NLRP3 inflammasome activation in gp120 LAV Tg mice. **a**–**e** Western blots (**a**) and densitometric analysis (**b**–**e**) of activated caspase-1 (Casp1-p20, **b**), cleaved IL-1β (IL-1β-p17, **c**), NLRP3 (**d**), and pro-IL-1β (**e**) in the cortex and hippocampus of WT ($n = 5$) and gp120 LAV Tg ($n = 5$) mice administered vehicle (PBS, 80 days) or MCC950 (10 mg/kg BW, dissolved in PBS, 80 days). **f** Brain sections of the cortex (upper panel) and hippocampus (lower panel) were immunostained with GSDMD, scale bar: 100 μM. **g**, **h** Images of immunolabeled GSDMD were analyzed quantitatively using ImageJ software. The Western blots and immunohistochemical results are representative of two independent experiments (**a**, **f**); data are displayed as the mean ± SEM ($n = 5$, **b**–**e**) and ($n = 6$, **g**, **h**) from two independent experiments. *$P <$ 0.05, **$P < 0.01$, ***$P < 0.001$; NS, no significance

that the protective effect of MCC950 was mainly driven by inhibition of microglial NLRP3 inflammasome activation. Collectively, these results suggest that the microglial NLRP3-dependent proinflammatory process is required for gp120 LAV-induced neuronal injury.

Gp120 Bal (CCR5-using) is more potent than gp120 LAV (CXCR4-using) in inducing NLRP3 inflammasome activation but not neurotoxicity

Because CCR5-using viruses have higher invasive activities in microglia than CXCR4-using viruses, we next compared the effect of CCR5-using gp120 (Bal) and CXCR4-using gp120 (LAV) in NLRP3 inflammasome activation and neurotoxicity. A caspase-1 activity assay showed that gp120 Bal was more potent in inducing caspase-1 activation than gp120 LAV when challenged at 24 or 48 h (Supplementary Fig. 6a). Consistent with this result, we found that gp120 Bal was also more effective than gp120 LAV in inducing ASC oligomer formation, caspase-1 activation, pyroptosis and IL-1β release (Supplementary Fig. 6b-e). These actions were significantly inhibited by MCC950 pretreatment, indicating that gp120 Bal is more potent in inducing NLRP3 inflammasome activation than gp120 LAV. In contrast, the neurotoxicity assay showed that gp120 LAV resulted in significantly lower neurite length than gp120 Bal (Supplementary Fig. 6f, g). These results suggested that gp120 Bal is more potent than gp120 LAV in inducing NLRP3 inflammasome activation but not neurotoxicity. Furthermore, we found that the V3 loop of gp120 Bal was more effective than gp120 LAV and gp120 SF2 (CCR5-CXCR4 dual tropism) in inducing microglial NLRP3 inflammasome activation (Supplementary Fig. 7a–e).

MCC950 blocks NLRP3 inflammasome activation in gp120 LAV Tg mice

NLRP3 is required for gp120 LAV-induced neurotoxicity in vitro. We next sought to extend these observations in vivo using gp120 LAV Tg mice, which is a good animal model for the development of treatment strategies for HAND.[5,31] We first determined whether MCC950 treatment inhibits NLRP3 inflammasome activation in the cortex and hippocampus because they were the main affected areas in the brains of gp120 LAV Tg mice.[5] Western blotting showed that the vehicle-treated gp120 LAV Tg mice exhibited higher expression of NLRP3 inflammasome components in both the cortex and hippocampus than did vehicle-treated and MCC950-treated WT mice (Fig. 6a). Chronic treatment with MCC950 reduced the levels of active caspase-1 and mature IL-1β both in the cortex and hippocampus of gp120 LAV Tg mice (Fig. 6a). Quantitative analysis showed a significant reduction of Casp-1-p20 and IL-1β-p17 in gp120 LAV Tg mice after MCC950 treatment (Fig. 6b, c). Immunohistochemical staining showed that vehicle-treated gp120 LAV Tg mice had higher GSDMD immunoreactivity in the brain than vehicle-treated and MCC950-treated WT mice, while treatment with MCC950 decreased this signal in gp120 LAV Tg mice (Fig. 6f–h). Moreover, the results of in situ immunofluorescence staining showed that treatment with

MCC950 significantly reduced the counts of Casp-1$^+$/Iba-1$^+$ and GSDMD$^+$/ Iba-1$^+$ cells in the brain sections of gp120 LAV Tg mice (Supplementary Fig. 3c, d). Interestingly, we observed that MCC950 did not significantly influence the expression of NLRP3 and pro-IL-1β (Fig. 6d, e), indicating that MCC950 has no effect on the priming stage of gp120 LAV-induced NLRP3 inflammasome activation. Together, these data suggested that treatment with MCC950 blocked cerebral NLRP3 inflammasome activation in gp120 LAV Tg mice.

Treatment with MCC950 ameliorates neuroinflammation, promotes M2 microglial polarization and inhibits the infiltration of effector immune cells in gp120 LAV Tg mice

We next analyzed whether treatment with MCC950 suppressed gp120 LAV-induced neuroinflammation. The results of immunohistochemical staining showed that vehicle-treated gp120 LAV Tg mice exhibited stronger immunoreactivity of GFAP, vimentin (astrocyte activation marker), and Iba-1 (microglia activation marker) in both the cortex and hippocampus than vehicle-treated and MCC950-treated WT mice (Fig. 7a–f, Supplementary Fig. 8). Administration of MCC950 observably reduced these immunopositive signals in the gp120 LAV Tg mice, indicating an obvious inhibitory effect of MCC950 on gp120 LAV-induced astrocytosis and microgliosis.

When activated, microglia can be divided into either a pro- or anti-inflammatory subtype, a process known as M1 and M2 microglia polarization, respectively. M1 microglia exert proinflammatory activity, while M2 microglia have an anti-inflammatory function.[32] We then investigated whether treatment with MCC950 promotes activated microglia polarization to an anti-inflammatory functional phenotype. Western blotting and ELISAs showed that the markers of M2-polarized microglia, including arginase-1, resistin-like molecule alpha (RELM alpha) and IL-4, all displayed higher expression in the brains of MCC950-treated gp120 LAV Tg mice than those of vehicle-treated Tg mice (Fig. 7g, h, i, k). Correspondingly, the expression of the M1-polarized microglial marker inducible nitric oxide synthase (iNOS) was suppressed in MCC950-treated gp120 LAV Tg mice (Fig. 7g, j). These data suggested that treatment with MCC950 results in a transition of proinflammatory microglia towards an anti-inflammatory state. Furthermore, we found that treatment with MCC950 not only suppressed the release of IL-1β but also other important proinflammatory mediators, including TNF-α, NO, COX-2, CCL3, and MCP-1, in the brains of gp120 LAV Tg mice **(**Fig. 7l–q**)**. Corresponding to the reduced chemokines (Fig. 7p, q), the infiltration of effector immune cells, including CD4$^+$ and CD8$^+$ T cells and activated monocytes (Ly6C$^+$), as well as the expression of complement C1q, was significantly suppressed in gp120 LAV Tg mice treated with MCC950 (Supplementary Fig. 9a-e). Taken together, these results indicated that treatment with MCC950 ameliorates neuroinflammation, inhibits effector immune cell infiltration and confers an anti-inflammatory M2 microglial phenotype in gp120 LAV Tg mice.

MCC950 alleviates neuronal death and promotes neuronal regeneration in gp120 LAV Tg mice

The extent of neuronal death was assessed using immunostaining for neuronal nuclear antigen (NeuN). Our results showed that MCC950-treated gp120 LAV Tg mice exhibited more neurons in both the cortex and hippocampus than vehicle-treated Tg mice (Fig. 8a–c). The results of in situ immunofluorescence staining showed that vehicle-treated gp120 LAV Tg mice exhibited significantly higher GSDMD and IL-1β immunoreactivity than vehicle- or MCC950-treated WT mice, as well as higher expression of GSDMD and IL-1β and lower NeuN$^+$ cell counts (Supplementary Fig. 10a, b). Treatment with MCC950 increased the NeuN$^+$ cell counts and decreased the expression of GSDMD and IL-1β in gp120 LAV Tg mice. Furthermore, a BrdU-labeling assay showed that MCC950 enhanced the counts of BrdU$^+$-NeuN$^+$ double-labeled neurons in gp120 LAV Tg mice, indicating that treatment with MCC950 promotes neuronal regeneration (Supplementary Fig. 11a, b).

The results of immunohistochemical staining of MAP-2 and synaptophysin indicated that vehicle-treated gp120 LAV Tg mice exhibited more severe dendritic damage and presynaptic loss in both the cortex and hippocampus than vehicle- and MCC950-treated WT mice (Fig. 8d, g). These neuropathological changes in the gp120 LAV Tg mice were largely reversed after treatment with MCC950 (Fig. 8d, g). Quantitative analysis showed that the brain sections of MCC950-treated gp120 LAV Tg mice showed significant increases in neuropils indicated by MAP-2 and synaptophysin compared with vehicle-treated Tg mice (Fig. 8e, f, h, i). Collectively, these data demonstrated that treatment with MCC950 ameliorates neuropathological deficits in gp120 LAV Tg mice.

MCC950 improves cognitive function in gp120 LAV Tg mice

To determine whether the abovementioned neuropathological changes were reflected in neurocognitive impairment, we evaluated the spatial learning ability, memory and behavioral abnormalities of the mice using the Morris water maze analysis and open field test. Overall, during the hidden-platform training, mice in all four groups showed a gradual decline in latency to find the hidden platform (Fig. 9a, b), while vehicle-treated gp120 LAV Tg mice needed more time and a longer distance to find the platform than did vehicle-treated and MCC950-treated WT mice (Fig. 9a, b). The increased time and distance needed by gp120 LAV Tg mice to find the hidden platform was not due to a slower swim speed (Fig. 9d). Administration of MCC950 significantly reduced the time and distance of gp120 LAV Tg mice to find the platform (Fig. 9a, b). After training, all mice were subjected to probe testing to assess memory. In addition, the swim speed and total distance in all groups were not significantly different (Fig. 9e, f), but the number of target platform crossings was significantly lower in vehicle-treated gp120 LAV Tg mice than in MCC950-treated Tg mice (Fig. 9g). Furthermore, we observed that MCC950-treated gp120 LAV Tg mice spent significantly more time searching in the platform quadrant (Q2) than the averaged time spent in all other quadrants, while vehicle-treated Tg mice spent markedly increased time in the non-platform quadrants (Fig. 9h). Representative tracks are exhibited in Fig. 9c, which showed that vehicle-treated WT, MCC950-treated WT and MCC950-treated gp120 LAV Tg mice made intensive searches in the target quadrant (Q2), whereas vehicle-treated gp120 LAV Tg mice had poorly focused search strategies. Altogether, these results suggested that treatment with MCC950 reversed the spatial and working memory deficits in the gp120 LAV Tg mice.

Finally, we assessed the spontaneous exploratory and anxiety-like behaviors of our mice in the open field area. We found that there was no substantial difference in the total distance moved by all mice (Fig. 9i), but the vehicle-treated gp120 LAV Tg mouse group spent less time and moved a shorter distance in the central area than did the other groups (Fig. 9j, l). The number of central area entries was also lower in vehicle-treated gp120 LAV Tg mice (Fig. 9m). This lack of central area exploration is displayed visually in the representative tracks shown in Fig. 9k. In rodents, an increase in fear response has been associated with an increase in the frequency of defecation.[33] We noted that the vehicle-treated gp120 LAV Tg group showed a higher defecation frequency than the other three groups (Fig. 9n), indicating that MCC950 provoked a diminished fear and stress response in gp120 LAV Tg mice. Collectively, these results suggested that treatment with MCC950 rescued anxiety-like behaviors and stress responses in gp120 LAV Tg mice.

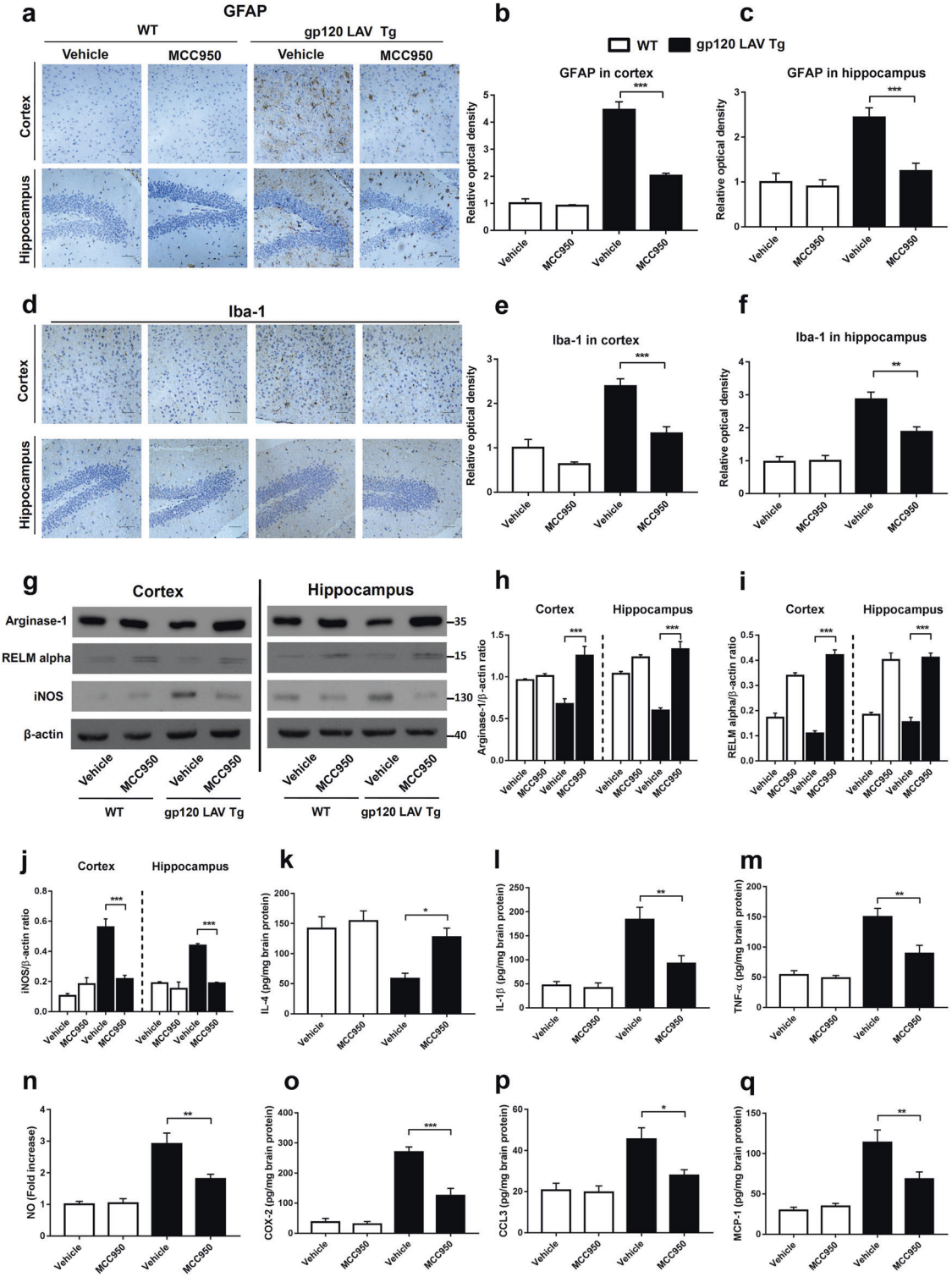

Fig. 7 Effect of MCC950 on neuroinflammation and microglia polarization in gp120 LAV Tg mice. Brain sections of WT ($n = 3$) and gp120 LAV Tg ($n = 3$) mice chronically administered vehicle (PBS, 80 days) or MCC950 (10 mg/kg BW, dissolved in PBS, 80 days) were assessed for the degree of neuroinflammation. Serial brain sections of the cortex (upper panels) and hippocampus (lower panels) were immunostained with GFAP (**a**) and Iba-1 (**d**) and analyzed quantitatively using ImageJ software (**b**, **c**, **e**, **f**). Scale bar: 100 μm. **g**–**j** Western blots (**g**) and densitometric analysis of arginase-1 (**h**), RELM alpha (**i**), and iNOS (**j**) in the cortex and hippocampus of WT ($n = 5$) and gp120 LAV Tg mice ($n = 5$) administered vehicle or MCC950. **k**–**q** Production of IL-4 (**k**), IL-1β (**l**), TNF-α (**m**), NO (**n**), COX-2 (**o**), CCL3 (**p**), and MCP-1 (**q**) in brain tissue homogenates of WT ($n = 6$) and gp120 LAV Tg ($n = 6$) mice treated with vehicle or MCC950. Data are displayed as the mean ± SEM ($n = 5$, **h**–**j**) and ($n = 6$, **b**, **c**, **e**, **f**, **k**–**q**) are from two independent experiments. The immunohistochemical staining and Western blot results are representative of two independent experiments (**a**, **d**, **g**). $^{*}P < 0.05$, $^{**}P < 0.01$, $^{***}P < 0.001$

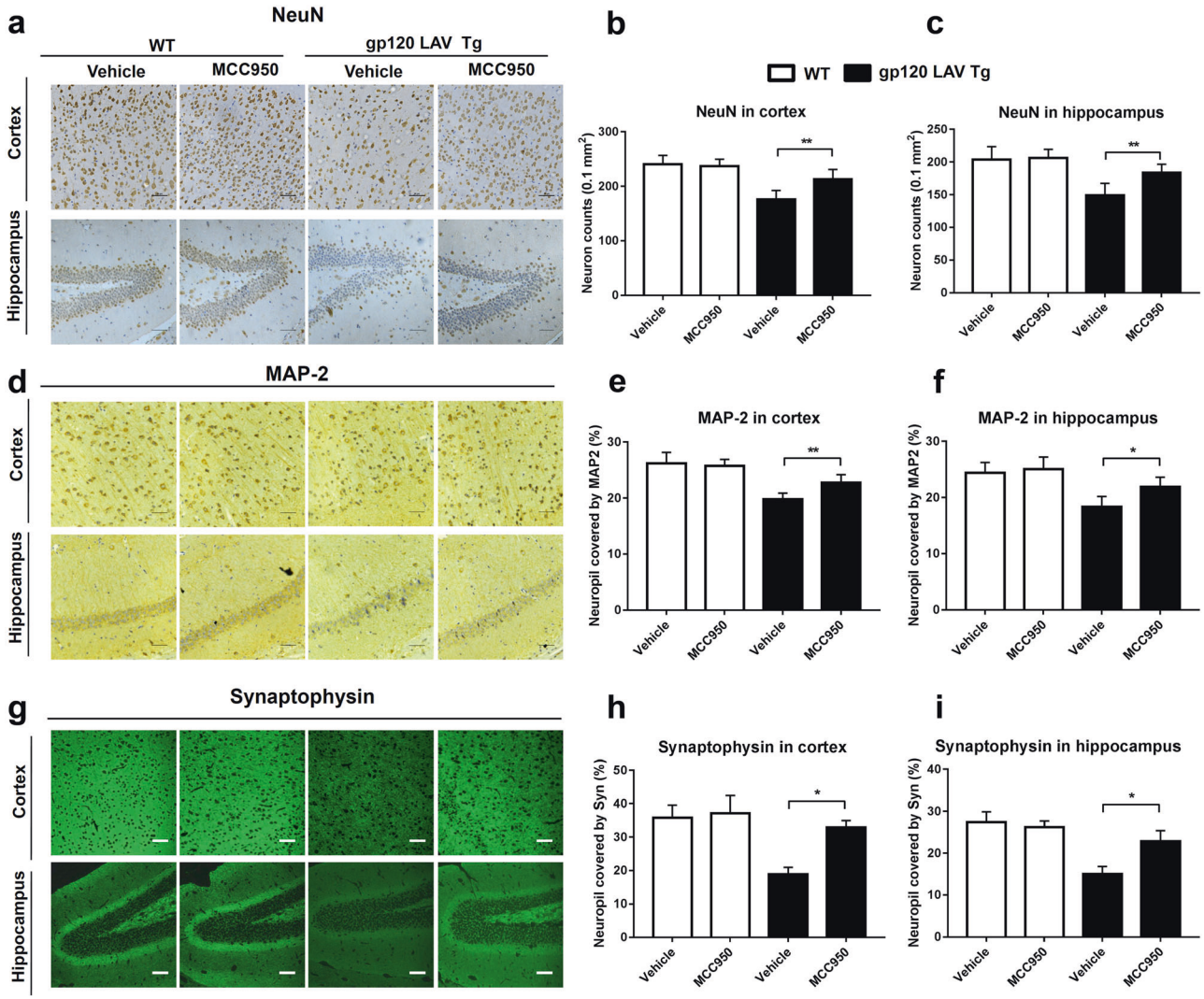

Fig. 8 Effect of MCC950 on neuronal damage in gp120 LAV Tg mice. **a**, **d** Representative images of the cortex (upper panels) and hippocampus (lower panels) immunolabeled with NeuN (**a**), MAP-2 (**d**), and synaptophysin (**g**) from WT ($n = 3$) and gp120 LAV Tg ($n = 3$) mice administered vehicle (PBS, 80 days) or MCC950 (10 mg/kg BW, dissolved in PBS, 80 days). **b**, **c**, **e**, **f**, **h**, **i** Quantification of microscopy data obtained in the cortex and hippocampus: quantification of NeuN-positive cells (counts/0.1 mm^2) in the cortex (**b**) and hippocampus (**c**); MAP-2 and synaptophysin represented by the percentage of positive neuropils. Scale bar: 100 μm. The immunohistochemical staining results are representative of two independent experiments (**a**, **d**, **g**). The data are displayed as the mean ± SEM ($n = 6$) from two independent experiments (**b**, **c**, **e**, **f**, **h**, **i**). *$P < 0.05$, **$P < 0.01$

DISCUSSION

In the present study, we showed that gp120 LAV induces neuroinflammation via NLRP3 inflammasome activation, which requires the CXCR4-Kv1.3 pathway, and that the NLRP3/IL-1β axis plays a pivotal role in mediating the neurotoxic response of gp120 LAV in vitro. We further confirmed the essential role of NLRP3 in gp120 LAV neuropathogenesis in vivo through the pharmacological inhibition of NLRP3 in gp120 LAV Tg mice by MCC950, a specific NLRP3 inhibitor, which resulted in reduced neuroinflammation, alleviated neuronal death and improved neurocognitive function. Together, these data indicated that NLRP3 might be a novel target for the treatment of HAND.

Our data contribute to the understanding of the pathogenesis of gp120-induced neuropathology, which is complicated and remains largely unknown. At least two mechanisms have been proposed to explain gp120 neuropathogenesis: "direct injury" and "bystander injury".[9] "Direct injury" refers to gp120 causing direct injury to neurons, while in "bystander injury," gp120 exerts neuronal toxicity via the inflammatory processes. Although these mechanisms might coexist, the bystander theory is more consistent with the existing data.[9] In this theory, gp120, which is shed by HIV-1 and/or infected macrophages/microglia, can activate neuroimmune cells, mostly microglia, leading to the release of proinflammatory cytokines, chemokines and excitotoxins. These factors mediate the neurotoxic effect, resulting in neuronal death and dysfunction.[6,9] However, how gp120 triggers the production of neurotoxin-associated factors is unclear. Here, for the first time, we showed that the NLRP3-IL-1β axis is the upstream mediator involved in the gp120-induced production of critical proinflammatory and neurotoxic factors. The pivotal role of the NLRP3 inflammasome in gp120 neuropathogenesis was further confirmed using a NLRP3-specific inhibitor and gp120 LAV Tg mice. Based on these findings, a proposed mechanism of gp120 neuropathogenesis is summarized in Fig. 10. Most importantly, a new neuropathological mechanism was elucidated here in which gp120 can induce neuronal pyroptosis. Pyroptosis is a type of programmed cell death that is distinct from apoptosis because pyroptosis not only leads to cell death but also triggers a

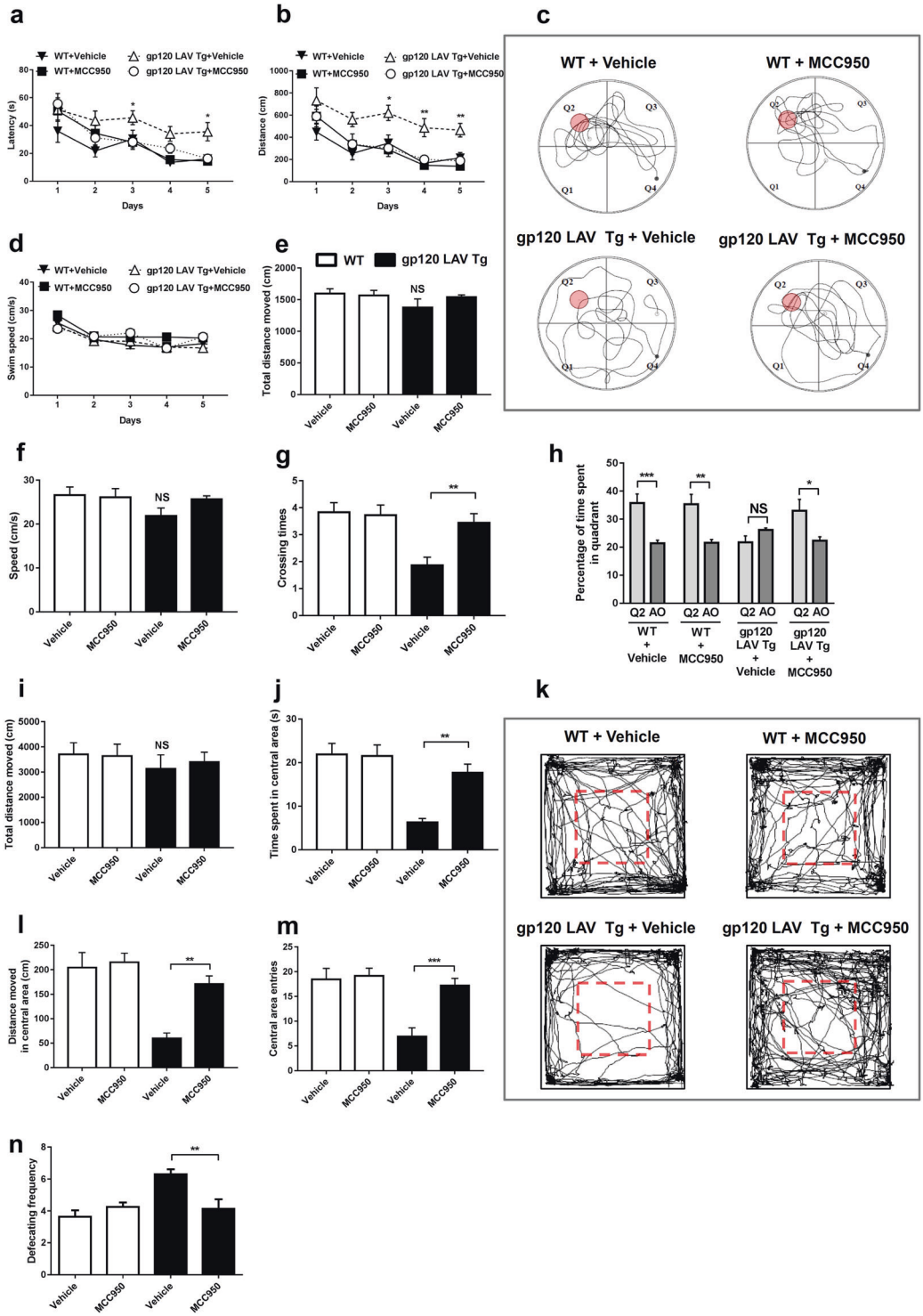

Fig. 9 Effect of MCC950 on learning deficits and behavioral alterations in gp120 LAV Tg mice. WT ($n = 24$, divided into vehicle, $n = 12$, and MCC950, $n = 12$) and gp120 LAV Tg ($n = 24$, divided into vehicle, $n = 12$, and MCC950, $n = 12$) mice were administered vehicle (PBS, 80 days) or MCC950 (10 mg/kg BW, dissolved in PBS, 80 days) and were subjected to the Morris water maze and open field tests. **a**, **b**, **d** Mean latency (**a**), travel distance (**b**), and swim speed (**d**) in the Morris water maze analysis during hidden-platform training. **c** Representative traces of mice during the probe trials. **e**–**h** Total travel distance (**e**), mean swim speed (**f**), annulus crossings (**g**), and time spent in the quadrants (**h**) of mice in the Morris water maze analysis during the probe trial; time spent in all other quadrants was averaged (AO) (**h**). **i**–**n** Spontaneous exploratory activity was analyzed using an open field apparatus. Total distance moved (**i**), time spent in the central area (**j**), distance moved in the central area (**l**), central area entries (**m**), and defecation frequency (**n**) in the open field apparatus were assessed over 15 min. **k** Representative traces of individual mice over 15 min in the open field arena. The data are displayed as the mean ± SEM ($n = 12$) from two independent experiments (**a**, **b**, **d**–**j**, **l**–**n**). $^{*}P < 0.05$, $^{**}P < 0.01$, $^{***}P < 0.001$. NS, no significance

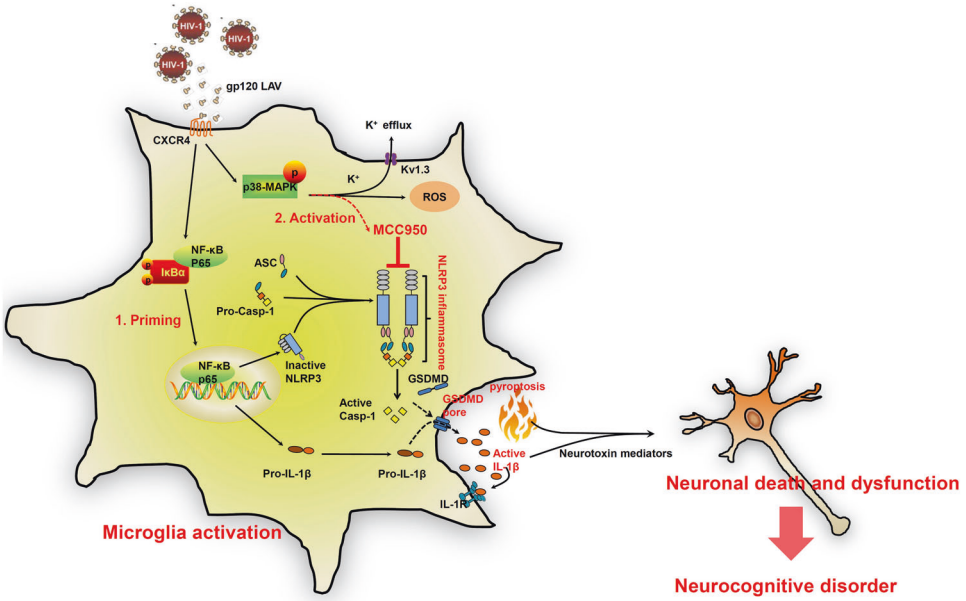

Fig. 10 A proposed schematic of gp120 LAV-mediated NLRP3 inflammasome activation, pyroptosis, neuroinflammation and neuronal death. During HIV-1 infection, gp120 LAV was shed from HIV-1 and/or infected macrophages/microglia. The binding of gp120 LAV to CXCR4 causes both NF-κB activation and K^+ efflux. NF-κB activation induces the transcription and expression of NLRP3 and pro-IL-1β, and K^+ efflux triggers NLRP3 inflammasome assembly, caspase-1 activation, pyroptosis and IL-1β release. Microglial pyroptosis further amplifies inflammatory reactions to release IL-1β. Extracellular IL-1β induces microglial activation and the upregulation of neuroinflammatory cytokines and neurotoxic mediators, resulting in neuronal death and dysfunction. MCC950 inhibits microglial NLRP3 inflammasome activation and provides a neuroprotective effect against gp120 LAV-induced neuronal death and dysfunction

cascade of inflammatory responses. In the in vitro study, we found that gp120 induces microglial pyroptosis and the release of ASC pyroptosomes (Supplementary Fig. 1). These extracellular ASC specks have the potential to further amplify the pyroptosis of neighboring cells.[34] We thus believe that gp120 can induce neuronal pyroptosis by itself or via activated microglia. Studies are underway to define this neuropathological mechanism of gp120.

An interesting discovery here is that Kv1.3, a member of the Shaker family of potassium channels, is implicated in gp120 LAV-induced NLRP3 inflammasome activation. A previous study demonstrated that Kv1.3-mediated K^+ efflux is critical in gp120 LAV-induced neuronal death,[27,28] but the downstream signaling pathways activated by K^+ efflux remain unknown. Here, we found that NLRP3 inflammasome activation is "downstream" of Kv1.3-mediated K^+ efflux, implying that gp120 LAV uses a newly identified Kv1.3 pathway to activate the NLRP3 inflammasome. This pathway is distinguished from most NLRP3 inflammasome activation routes induced by viruses, for example HIV-1 Tat, influenza virus M2 protein, prion protein and hepatitis C virus,[35–38] which are mainly mediated by the phagolysosomal pathway, as inhibiting phagolysosomal activity did not impact the inflammasome activation induced by gp120 LAV. Kv1.3 has already been reported to be involved in many NLRP3 inflammasome-associated diseases, such as obesity, type-1 diabetes mellitus, atherosclerosis, rheumatoid arthritis, multiple sclerosis and Alzheimer's disease,[39–42] but evidence linking Kv1.3 to the NLRP3 inflammasome is lacking. We speculate that Kv1.3 may play a more significant role in neurodegenerative diseases than in other diseases because Kv1.3 is highly expressed in the CNS and acts as a key regulator of microglial function.[43] Further clarification of the relationship between the Kv1.3 and the NLRP3 inflammasome, especially in the context of neurodegenerative diseases, may deepen our theoretical and clinical understanding of these challenging disorders.

IL-1β is an important proinflammatory cytokine that mediates the neurotoxic effect of gp120 described here. However, the question remains: is IL-1β a good target for intervention in gp120-induced neuropathology? The answer may be no. Although numerous studies have described the neurotoxicity of IL-1β, there is also evidence supporting the potential neuroprotective effects of this cytokine.[44] A series of data suggest that a high concentration of IL-1β exerts a neurotoxic effect but that a low concentration of IL-1β could enhance neuronal survival.[45] The neuroprotective effects of IL-1β might be exerted via several mechanisms, including suppression of glutamate release and Ca^{2+} influx, enhancement of nerve growth factor and neurotrophin production.[44–47] Indeed, a previous study has reported that IL-1β may prevent gp120-induced neuronal apoptosis by regulating nerve growth factor release.[48] Thus, directly targeting IL-1β might not always be beneficial. In addition to caspase-1, gp120-induced IL-1β processing may be controlled by other mediators, such as matrix metalloproteinase 9.[49] Thus, specifically targeting NLRP3 rather than IL-1β may be a better therapeutic strategy for gp120-induced neuropathology because the specific blocking of NLRP3 would not lead to the complete inhibition of IL-1β production, and the neuroprotective effect may remain intact. This scenario may explain why treatment with MCC950 promoted neurogenesis and improved neurocognitive deficits in gp120 LAV Tg mice. Thus, we propose that targeting NLRP3 rather than IL-1β is a better strategy for the intervention of gp120-induced neuropathology.

Although we found that MCC950 is useful in the context of gp120-induced neuronal dysfunction, is this agent also suitable for HAND intervention? Microglia play a pivotal role in the pathogenesis of HAND. Microglia are the primary immune effector cells in the brain and can be activated by a variety of foreign substances.[10] Regardless of whether they are exposed to HIV-1 or gp120, activated microglia are the key drivers of neuronal dysfunction because numerous studies have reported that the severity of HIV dementia is more correlated with the degree of microglial activation than the HIV-1 load or the number of HIV-1-infected cells in the CNS.[50,51] In the present study, we found that treatment with MCC950 reduced microglial activation and promoted the M1 microglial phenotype switch to M2. These

findings suggest that MCC950 may also be suitable for the treatment of HAND. Moreover, recent studies have shown that MCC950 can cross the blood brain barrier.[17,52] Because a lack of anti-inflammatory properties and poor blood brain barrier permeability are the major limitations of the currently used antiretroviral agents,[53] we speculated that MCC950 may be very useful for treating HAND in combination with ART.

Several issues should be discussed here. First, the transgenic mouse model used here expresses high levels of gp120, and thus, the conclusion of this study may only be relevant in pre-ART-era patients with HIV-1 dementia. Many recent studies have shown that the brains of gp120 LAV Tg mice and neuroAIDS patients share a significant number of features, including activation of innate immunity, differentially regulated genes, changes in cellular signaling pathways, disturbed neurogenesis, and learning deficits. The continued relevance of the gp120 LAV Tg mouse model is supported for studies on HIV infection of the CNS, neuroAIDS, and HAND.[31] The second issue is the limited generalizability of gp120, which was obtained from CXCR4-using HIV-1 variants here. The rationale for selecting gp120 LAV here is maintaining consistency with the gp120 LAV Tg mice.[5] CXCR4-using gp120 causes significant neuronal death, whereas CCR5-using gp120 exerts neurotoxic effects and promotes the release of brain-derived neurotrophic factor.[54,55] These findings may explain why gp120 Bal was more potent in inducing NLRP3 inflammasome activation, but not neurotoxicity, than gp120 LAV. Although CXCR4-using isolates often determine progression to AIDS- and HIV-1-associated dementia, most of the CNS HIV-1 isolates are CCR5-using strains rather than CXCR4-using strains.[9,10] Furthermore, CCR5-using viruses were more efficient than CXCR4-using strains in invading macrophages/microglia.[10] Thus, exploring the mechanism of CCR5-using gp120-induced neuronal death may provide new insights for future investigations of the pathogenesis of HAND. The last issue is the role of vimentin in gp120-induced neuropathology. In the present study, we found that vimentin, an astrocytic marker, is more highly expressed in gp120 LAV Tg mice than WT mice. Vimentin is not only an astrocytic marker and an intermediate filament cytoskeletal protein but also an important signal molecule. Vimentin has been reported to mediate many biological and pathogenic processes, including epithelial–mesenchymal transition, NF-κB and NLRP3 inflammasome activation, neurodegenerative disease, and atherosclerosis.[56–60] More interestingly, previous studies showed that vimentin could interact with the V3 loop of gp120 and upregulate NF-κB-mediated signaling through its head domain.[57,61] We further found that vimentin deficiency prevents neuronal damage and behavioral impairment in gp120 LAV Tg mice (unpublished results). The question remains of how to *further* explore the regulatory role of vimentin in gp120 LAV-induced neuropathology. Answering this question may provide novel therapeutic targets for HAND.

In summary, our data showed that gp120-induced microglial NLRP3 inflammasome activation, pyroptosis and IL-1β release, which initiated neuroinflammation and ultimately led to neuronal death and behavioral impairment. Based on these data, we showed that administration of MCC950 has a neuroprotective effect on gp120 LAV Tg mice. In light of the anti-inflammatory properties and good blood brain barrier permeability of MCC950, we believe that it may be effective in the treatment of HAND in combination with ART. Future studies are warranted to address the neuroprotective effects of MCC950 in an animal model that is more closely related to HAND in humans.

MATERIALS AND METHODS

Reagents and inhibitors

Full-length gp120 LAV and gp120 Bal were obtained from Protein Sciences (Meriden, CT). V1–V5 loops from HIV-1 LAV, the V3 loop from HIV-1 Bal and the V3 loop from HIV-1 SF2 were synthesized by GL Biochem (Shanghai), Ltd. Their amino acid sequences are listed in Table 1. Ultra-pure LPS K12 was purchased from Invitrogen (Toulouse, France). Cytochalasin D, bafilomycin A, and Z-YVAD-fmk were purchased from Merck (Darmstadt, Germany). BrdU, MTT, ATP, MitoTEMPO, disuccinimidyl suberate (DSS), NAC, ADPC, and glyburide were purchased from Sigma-Aldrich (USA). MCC950, AMD3100, PAP-1, and CA-074Me were purchased from MCE (MedChem Express, USA). IL-1RA was purchased from R&D (Minneapolis, MN, USA), and 1,1′-dioctadecyl-3,3,3′,3′-tetramethylindocarbocyanine perchlorate (DiI) was purchased from Beyotime Institute of Biotechnology, China.

Table 1. Amino acid sequence and purity of V3 loops used in this study

Peptides	Amino acid sequence	Purity
V3 loop-Bal	CTRPNNNTRKSIHIGPGRAFYTTGEIIGDIRQAHC	≥95%
V3 loop-SF2	CTRPNNNTRKSIYIGPGRAFHTTGRIIGDIRKAHC	≥95%
V3 loop-LAV	CTRPNNNTRKSIRIQRGPGRAFVTIGKIGNMRQAHC	≥95%
V1 loop-LAV	CTDLGNATNTNSSNTNSSSGEMMMEKGEIKN	≥95%
V2 loop-LAV	CSFNISTSIRGKVQKEYAFFYKLDIIPIDNDTTSYTLTSC	≥95%
V4 loop-LAV	CNSTQLFNSTWFNSTWSTEGSNNTEGSDTITLPC	≥95%
V5 loop-LAV	NGSEIFRPG	≥95%

Isolation and treatment of mouse primary microglia and neurons

Animal protocols were approved by the Medical Ethics Committee of Southern Medical University (Guangzhou, China) and performed at Southern Medical University according to the guidelines for the protection of animal subjects. All efforts were made to reduce the number of animals used and their suffering.

Mouse primary microglia were obtained from 10-day-old C57BL/6 mice by shaking the glial cultures, as described previously.[62] Immunostaining for Iba-1 was performed to detect the purity of the microglia. Isolated microglia were maintained in DMEM medium containing 10% heat-inactivated fetal bovine serum (FBS, PAN Biotech, Aidenbach, Germany), 5 μg/ml bovine insulin and 0.2% glucose. To detect the activation of the NLRP3 inflammasome, cells were stimulated with serum-free medium containing gp120 LAV or gp120 Bal (200 pM as described previously[63,64]) or variable loops (200 ng/ml) for 6–24 h. For the positive control, cells were prestimulated with 0.5 μg/ml LPS for 4 h and treated with serum-free medium containing 2 mM ATP for 20 h. After treatment, cells were lysed and assayed for the expression of NLRP3, pro-caspase-1, pro-IL-1β, and GSDMD using western blotting. Culture supernatants were divided into two portions. One portion was precipitated by 10% trichloroacetic acid and analyzed for the active form of caspase-1 and IL-1β using western blotting. The remaining portion was assessed for IL-1β, COX-2, and TNF-α concentrations by ELISAs (Proteintech Group, Chicago, USA). NO production was analyzed using the Griess reaction according to the method described in the NO assay kit (Beyotime Institute of Biotechnology, China). LDH release in culture supernatants was detected to assess the extravasation of cytoplasmic contents using the LDH Assay Kit (Pierce, Rockford, IL, USA).

Primary cortical neurons were isolated from C57BL/6 mice as previously described.[65] Neurons were seeded into collagen-coated 24-well plates and grown in Neurobasal Medium supplemented with 2% B27 (Gibco, USA) and 1% penicillin/streptomycin (HyClone, USA). To assess gp120-induced neuronal injury in vitro, primary microglia were stimulated with MCC950 for 2 h and incubated for 24 h with 200 pM gp120. Culture supernatants were harvested and ultrafiltered to clear the residual gp120 and applied to neurons for 72 h as described previously.[66,67] The

neuronal cultures were fixed, and neuronal damage was evaluated by immunofluorescence analysis using rabbit anti-MAP-2 (Proteintech Group, Chicago, USA) as described below. Neurite length was measured by NeuronJ (ImageJ add-on software) as described previously.[68]

Culture and treatment of microglial cell lines

The BV2 mouse microglial cell line was purchased from the National Infrastructure of Cell Line Resource (Beijing, China) and routinely cultured at 37 °C and 5% CO_2 in RPMI 1640 medium containing 10% heat-inactivated fetal bovine serum (FBS, PAN Biotech, Aidenbach, Germany), penicillin (100 units/ml, HyClone, USA), and streptomycin (100 μg/ml, HyClone, USA). To detect the activation of the NLRP3 inflammasome, we seeded BV2 at 5×10^5/ml into 96-well plates for ELISA and 5×10^6/ml into 6-well plates for western blotting analysis. The next day, the cells were stimulated with serum-free medium containing gp120 (0.5 μg/ml) or V1–V5 loops (200 ng/ml) for 6–24 h. For the positive control, BV2 cells were prestimulated with 1 μg/ml LPS for 4 h and treated with serum-free medium containing 2.5 mM ATP for 20 h. For the experiments studying the effect of inhibitor on gp120 LAV-induced inflammasome activation, the cells were prestimulated with Z-YVAD-fmk (5–20 μM), MCC950 (1–25 μM), AMD3100 (0.1–10 μM), PAP-1 (0.1–2 μM), glyburide (50–200 μM), ADPC (5–50 μM), NAC (5–25 μM), MitoTEMPO (100–500 μM), bafilomycin A (10–200 nM), cytochalasin D (1–25 μM), or CA-074Me (5–20 μM) for 30 min–2 h before stimulation with gp120 for 24 h. To inhibit the K^+ efflux, BV2 cells were cultured with a high concentration of KCl (50–200 mM). Sample preparation and analysis were performed as described above.

For siRNA-mediated knockdown, predesigned siRNAs specific for NLRP1, NLRP3, AIM2, NLRC4, CXCR4, and Kv1.3 and nontargeting control siRNA were obtained from Dharmacon Research, Inc. (Lafayette, CO, USA). Lipofectamine 3000 transfection reagent (Invitrogen, USA) was used to transfect BV2 cells with siRNAs according to the supplier's recommendations. Afterward, the cells were cultured for an additional 48 h to allow robust knockdown of protein before experiments were carried out.

Animal model and treatment

WT mice and transgenic mice expressing soluble gp120 LAV using the modified GFAP promoter were described previously.[5] All mice were specific pathogen free and kept in the animal facility under a strict 12 h light/dark cycle. To investigate the inhibitory effect of Z-YVAD-fmk on gp120-induced IL-1β production in vivo, WT and gp120 LAV Tg mice (10–12 months) were randomly divided into four groups: WT + vehicle ($n = 5$), WT + Z-YVAD-fmk ($n = 5$), gp120 LAV Tg + vehicle ($n = 5$), and gp120 LAV Tg + Z-YVAD-fmk ($n = 5$). Mice were intraperitoneally injected with 200 μl sterile PBS (vehicle, containing 1% vol/vol DMSO) or Z-YVAD-fmk [10 mg/kg body weight (BW), dissolved in 1% vol/vol DMSO in PBS] every second day for 30 days. Afterward, all mice were euthanized by asphyxiation with CO_2, and the brains were removed and homogenized in radioimmunoprecipitation assay (RIPA) lysis buffer containing protease inhibitors and immediately centrifuged at 20,000 × *g* for 10 min at 4 °C. The supernatants were harvested and measured for IL-1β release using ELISA and Western blotting. To evaluate the neuroprotective effect of MCC950 against gp120-induced neuropathology in vivo, WT and gp120 LAV Tg mice (11–12 months) were randomly divided into four groups: WT + vehicle ($n = 8$–12), WT + MCC950 ($n = 8$–12), gp120 LAV Tg + vehicle ($n = 8$–12), and gp120 LAV Tg + MCC950 ($n = 8$–12). Mice were intraperitoneally injected with sterile 200 μl PBS (vehicle) or MCC950 (10 mg/kg BW in PBS) every third day for 80 days. The spatial learning, memory and behavioral abnormalities were examined using a Morris water maze analysis and open field test. Finally, mice were humanely euthanized by asphyxiation with CO_2. The brain was removed and divided into two hemispheres; one portion was fixed in 10% formaldehyde, embedded in paraffin and sectioned for immunohistochemical staining. The cortex and hippocampus of the other portion were dissected and snap-frozen at −80 °C. For the determination of cytokines, individual brain cortical and hippocampal tissue samples were homogenized and lysed as mentioned above. The samples were harvested and measured for cytokine and chemokine concentrations by ELISAs (Proteintech Group, Chicago, USA).

Behavioral testing

Spatial learning and memory were evaluated using the Morris water maze as described previously.[16] The water maze apparatus is a circular tank (diameter 1.3 m, divided into four quadrants, called Q1, Q2, Q3, Q4) filled to 30 cm with 22–24 °C opacified water and containing a hidden platform (2–3 cm below the water surface, diameter 15 cm) at the center of Q2. First, animals were trained to find the platform for five consecutive days (four trials/day), orienting by three external cues surrounding the water tank as spatial references. The mice were released into the water facing the edge of the tank from one of four randomized positions, and each position was used once each day. Mice had 120 s to search for the platform in one trial; if the mice did not climb up the platform, they were manually placed on it. Animal movements were tracked by using a TSE VideoMot2 video tracking system (TSE Systems GmbH, Bad Homburg, Germany). After the hidden-platform training, the platform was removed, and the mice had 60 s to search for the pool. The total distance moved, swim speed, time spent in each quadrant and number of platform location crossings were analyzed.

The open field assay was carried out as described previously.[16] The open field apparatus is a square box (40 × 40 × 30 cm high) containing a central square (20 × 20 cm). Individual mice were released into the corner of the open field apparatus, and their behavior was recorded for 15 min by a TSE VideoMot2 video tracking system. The total distance moved, distance moved in the central area, time spent in the central area and number of central area entries were analyzed. The frequency of defecation was manually recorded and was defined as the number of times a mouse defecates in the open field area during the observation period. The dimension of stool >1 cm was counted.

Western blotting

Cells were lysed directly by 100 μl of 1 × SDS-PAGE loading buffer. Cell lysates were separated using SDS-PAGE and transferred onto polyvinylidene difluoride membranes (pore size, 0.45 μm, Millipore, USA). Then, the membranes were blocked with 5% (wt/vol) nonfat milk in TBST buffer [50 mM Tris/HCl, pH 7.4–7.6, 150 mM NaCl and 0.1% (vol/vol) Tween-20] for 1 h, followed by incubation in primary antibody diluted in 5% (wt/vol) nonfat milk-TBST for 12 h at 4 °C. Afterward, the membranes were incubated with the appropriate horseradish peroxidase (HRP)-conjugated secondary antibody diluted in 5% (wt/vol) nonfat milk-TBST for 1 h. The expression of antigen was visualized using an enhanced chemiluminescence reagent kit (Bio-Rad Laboratories, USA).

The primary antibodies used are as follows: rabbit anti-IL-1β (1:2000), rabbit anti-arginase-1 (1:1000), rabbit anti-NF-κB p65 (1:50,000), rabbit anti-RELM alpha (1:3000), rabbit anti-CXCR4 (1:1000), rabbit anti-NLRP1 (1:1000), and rabbit anti-NLRP3 (1:1000) were all purchased from Abcam (Cambridge, USA); rabbit anti-caspase-1 (1:2000), rabbit anti-AIM2 (1:2000), rabbit anti-IκBα (1:2000), rabbit anti-GSDMD (1:2000), rabbit anti-Histone H3 (1:6000), and rabbit anti-Kv1.3 (1:2000) were all purchased from Proteintech Group (Chicago, USA); rabbit anti-β-actin (1:6000) (Bioss Antibodies, USA); mouse anti-ASC (1:200) (Santa Cruz Biotechnology, USA) were used; rabbit anti-NLRC4 (1:800) and rabbit anti-iNOS (1:800) were purchased from Boster Biotechnology (Wuhan, China); rabbit anti-cleaved-caspase-1 (1:1000), rabbit anti-cleaved-IL-1β (1:1000), rabbit anti-phospho-p38 MAPK

(Thr180/Tyr182) (1:1000), and rabbit anti-p38 MAPK (1:1000) were all purchased from Cell Signaling Technology (Danvers, USA).

ASC oligomerization and speckle formation

ASC oligomerization was detected as previously described.[25] In brief, cells were collected and lysed in ice-cold buffer (20 mM HEPES-KOH, pH 7.5, 1 mM EDTA, 1 mM EGTA, 1.5 mM $MgCl_2$, 10 mM KCl, 320 mM sucrose) using a 21-gauge needle. Cell lysates were centrifuged, and 30 µl supernatants were kept as input controls for western blot analysis. The pellets were crosslinked by the addition of 2 mM DSS and incubation for 30 min at room temperature. The crosslinked protein was centrifuged and resuspended in 50 µl of Laemmli sample buffer and boiled for western blot analysis.

ASC speckle formation was detected using immunofluorescence. After treatment, BV2 cells were fixed with 4% paraformaldehyde and permeabilized using 0.1% Triton X-100. The cells were blocked sequentially with 3% BSA for 1 h at room temperature, followed by incubation with mouse anti-ASC (1:200, Santa Cruz Biotechnology, USA) and fluorescein isothiocyanate (FITC)-conjugated anti-mouse IgG (1:2000, Abcam, USA). Then, 4′,6-diamidino-2-phenylindole (DAPI) and DiI were used to stain nuclei and membranes, respectively. The results were visualized under a fluorescence microscope (Nikon Eclipse: TE 2000-E, Japan).

Caspase-1 activity measurements

For the colorimetric method, caspase-1 activity was measured using a caspase-1 colorimetric assay kit (Beyotime Institute of Biotechnology, China) according to the manufacturer's instructions. This assay is based on spectrophotometric detection of the chromophore ρ-nitroanilide (ρNA) after cleavage from the labeled substrate acetyl-Tyr-Val-Ala-Asp ρ-nitroanilide (Ac-YVAD-ρNA) by activated caspase-1. In brief, 50 µg protein was mixed with 20 nmol Ac-YVAD-ρNA in a 96-well microtiter plate and incubated for 2 h at 37 °C. The production of ρNA was monitored at 405 nm using a microplate reader.

BrdU labeling

To detect neurogenesis, 50 mg/kg body weight of BrdU (Sigma-Aldrich, USA) was injected intraperitoneally. BrdU was injected three times a week, while animals were sacrificed 3 weeks post-injection. BrdU incorporation was analyzed by immunohistochemical staining (see below).

Immunohistochemistry

Paraffin sections were deparaffinized and rehydrated following standard protocols. To retrieve antigen, sections were boiled with 0.01 M citrate buffer (pH 6.0) for 30 min. Afterward, sections were washed and immersed in 3% hydrogen peroxide/methanol for 30 min at room temperature. Then, the sections were blocked with 1% BSA and incubated with the following primary antibodies: rabbit anti-GSDMD (1:400) and rabbit anti-MAP-2 (1:400) were purchased from Proteintech Group (Chicago, USA), and rabbit-Iba-1 (1:250), rabbit anti-NeuN (1:400), rabbit anti-GFAP (1:400), and rabbit anti-vimentin (1:400) were all purchased from Abcam (Cambridge, USA). The sections were then washed, incubated with the appropriate secondary antibodies, washed and visualized using DAB (3,3-diaminobenzidine) with hematoxylin counterstaining. The optical density of the immunostained areas and the number of neurons with NeuN immunoreactivity were quantified using ImageJ software (US National Institutes of Health).

For the immunofluorescence method, the sections were blocked with 1% BSA and incubated with the following primary antibodies: rabbit anti-GSDMD (1:400) and rabbit anti-synaptophysin (1:200), all purchased from Proteintech Group (Chicago, USA); rabbit-Iba-1 (1:250), rabbit anti-NeuN (1:400) and mouse anti-BrdU (1:500), all purchased from Abcam (Cambridge, USA); and rabbit anti-cleaved-caspase-1 (1:200), purchased from Cell Signaling Technology (Danvers, USA). The sections were then washed and incubated with appropriate secondary antibodies and DAPI, followed by fluorescence microscopy (Nikon Eclipse: TE 2000-E, Japan) analysis.

Statistical analysis

Data are presented as the mean ± standard error (SEM). Analysis between two groups was performed by unpaired two-tailed Student's *t*-test. Analysis involving more than two groups was examined by two-tailed, one-way analysis of variance (ANOVA) with multiple comparison post hoc analysis. The data of escape latency, swim speed and distance moved to find the platform in the hidden-platform training stage of the water maze test were analyzed using two-tailed, two-way ANOVA (with treatment and time as factors). All statistical analyses were performed using GraphPad Prism software version 7.0. $P < 0.05$ was defined as statistically significant.

ACKNOWLEDGEMENTS

This project was financially supported by the Key Program of the Natural Science Foundation of Guangdong, China (No. 2017B030311017), the National Natural Science Foundation of China (No. 81370740), the Program of the Natural Science Foundation of Guangdong, China (No. 2018A030313845), and the China Postdoctoral Science Foundation (No. 2018M633076).

AUTHOR CONTRIBUTIONS

S.H., H.C., E.M., X.H., W.Y., and L.W. conceived and designed the experiments. M.E. and S.H. contributed reagents/materials/analysis tools. X.H., W.Y., Q.Z., Z.Z., Yi W., L.Q.L., L.T.L., Yu W., Z.G., J.G., H.Z., Y.L., S.Y., and T.H. performed the experiments and acquired and analyzed the data. X.H., W.Y., J.G., Q.Z., and Z.Z. prepared the figures and L.W., E.M., S.H., and H.C. helped revise them. X.H., S.H., H.C., W.Y., J.G., and L.W. drafted the paper, and S.H., X.H., E.M., H.C., W.Y., B.Z., L.L. and Yi W. revised it. All authors read and approved the final paper.

ADDITIONAL INFORMATION

The online version of this article (https://doi.org/10.1038/s41423-019-0260-y) contains supplementary material.

Competing interests: The authors declare no competing interests.

REFERENCES

1. Saylor, D. et al. HIV-associated neurocognitive disorder—pathogenesis and prospects for treatment. *Nat. Rev. Neurol.* **12**, 234–248 (2016).
2. Clifford, D. B. & Ances, B. M. HIV-associated neurocognitive disorder. *Lancet Infect. Dis.* **13**, 976–986 (2013).
3. Eggers, C. et al. HIV-1-associated neurocognitive disorder: epidemiology, pathogenesis, diagnosis, and treatment. *J. Neurol.* **264**, 1715–1727 (2017).
4. Brenneman, D. E. et al. Neuronal cell killing by the envelope protein of HIV and its prevention by vasoactive intestinal peptide. *Nature* **335**, 639–642 (1988).
5. Toggas, S. M. et al. Central nervous system damage produced by expression of the HIV-1 coat protein gp120 in transgenic mice. *Nature* **367**, 188–193 (1994).
6. Kaul, M., Garden, G. A. & Lipton, S. A. Pathways to neuronal injury and apoptosis in HIV-associated dementia. *Nature* **410**, 988–994 (2001).
7. Capo-Velez, C. M., Morales-Vargas, B., Garcia-Gonzalez, A. & Grajales-Reyes, J. G. The alpha7-nicotinic receptor contributes to gp120-induced neurotoxicity: implications in HIV-associated neurocognitive disorders. *Sci. Rep.* **8**, 1829 (2018).
8. D'Hooge, R., Franck, F., Mucke, L. & De Deyn, P. P. Age-related behavioural deficits in transgenic mice expressing the HIV-1 coat protein gp120. *Eur. J. Neurosci.* **11**, 4398–gp4402 (1999).
9. Gonzalez-Scarano, F. & Martin-Garcia, J. The neuropathogenesis of AIDS. *Nat. Rev. Immunol.* **5**, 69–81 (2005).
10. Chen, N. C., Partridge, A. T., Sell, C., Torres, C. & Martin-Garcia, J. Fate of microglia during HIV-1 infection: from activation to senescence? *Glia* **65**, 431–446 (2017).
11. Heneka, M. T., McManus, R. M. & Latz, E. Inflammasome signalling in brain function and neurodegenerative disease. *Nat. Rev. Neurosci.* **19**, 610–621 (2018).

12. Mangan, M. S. J. et al. Targeting the NLRP3 inflammasome in inflammatory diseases. *Nat. Rev. Drug Disco.* **17**, 588–606 (2018).
13. Liu, X. et al. Inflammasome-activated gasdermin D causes pyroptosis by forming membrane pores. *Nature* **535**, 153–158 (2016).
14. Song, L., Pei, L., Yao, S., Wu, Y. & Shang, Y. NLRP3 inflammasome in neurological diseases, from functions to therapies. *Front Cell Neurosci.* **11**, 63 (2017).
15. Allan, S. M., Tyrrell, P. J. & Rothwell, N. J. Interleukin-1 and neuronal injury. *Nat. Rev. Immunol.* **5**, 629–640 (2005).
16. Heneka, M. T. et al. NLRP3 is activated in Alzheimer's disease and contributes to pathology in APP/PS1 mice. *Nature* **493**, 674–678 (2013).
17. Gordon, R. & Albornoz, E. A. Inflammasome inhibition prevents alpha-synuclein pathology and dopaminergic neurodegeneration in mice. *Sci. Transl. Med* **10**, eaah4066 (2018).
18. Walsh, J. G. et al. Rapid inflammasome activation in microglia contributes to brain disease in HIV/AIDS. *Retrovirology* **11**, 35 (2014).
19. Kaul, M. & Lipton, S. A. Mechanisms of neuronal injury and death in HIV-1 associated dementia. *Curr. HIV Res.* **4**, 307–318 (2006).
20. Michael, N. L. & Moore, J. P. HIV-1 entry inhibitors: evading the issue. *Nat. Med.* **5**, 740–742 (1999).
21. Maung, R. et al. CCR5 knockout prevents neuronal injury and behavioral impairment induced in a transgenic mouse model by a CXCR4-using HIV-1 glycoprotein 120. *J. Immunol.* **193**, 1895–1910 (2014).
22. Sun, N.-N. et al. Mir-21 mediates the inhibitory effect of Ang (1–7) on AngII-induced NLRP3 inflammasome activation by targeting Spry1 in lung fibroblasts. *Sci. Rep.* **7**, 14369 (2017).
23. Doitsh, G. et al. Cell death by pyroptosis drives CD4 T-cell depletion in HIV-1 infection. *Nature* **505**, 509–514 (2014).
24. Ahmad, F. et al. Evidence of inflammasome activation and formation of monocyte-derived ASC specks in HIV-1 positive patients. *Aids* **32**, 299–307 (2018).
25. Coll, R. C. et al. A small-molecule inhibitor of the NLRP3 inflammasome for the treatment of inflammatory diseases. *Nat. Med.* **21**, 248–255 (2015).
26. Afonina, I. S., Zhong, Z., Karin, M. & Beyaert, R. Limiting inflammation-the negative regulation of NF-kappaB and the NLRP3 inflammasome. *Nat. Immunol.* **18**, 861–869 (2017).
27. Liu, J., Xu, C., Chen, L., Xu, P. & Xiong, H. Involvement of Kv1.3 and p38 MAPK signaling in HIV-1 glycoprotein 120-induced microglia neurotoxicity. *Cell Death Dis.* **3**, e254 (2012).
28. Xu, C. et al. HIV-1 gp120 enhances outward potassium current via CXCR4 and cAMP-dependent protein kinase A signaling in cultured rat microglia. *Glia* **59**, 997–1007 (2011).
29. Ogishi, M. & Yotsuyanagi, H. Prediction of HIV-associated neurocognitive disorder (HAND) from three genetic features of envelope gp120 glycoprotein. *Retrovirology* **15**, 12 (2018).
30. Barak, O. et al. Involvement of brain cytokines in the neurobehavioral disturbances induced by HIV-1 glycoprotein120. *Brain Res.* **933**, 98–108 (2002).
31. Thaney, V. E. et al. Transgenic mice expressing HIV-1 envelope protein gp120 in the brain as an animal model in neuroAIDS research. *J. Neurovirol.* **24**, 156–167 (2018).
32. Ransohoff, R. M. A polarizing question: do M1 and M2 microglia exist? *Nat. Neurosci.* **19**, 987–991 (2016).
33. Andersen, I. L., Boe, K. E., Foerevik, G., Janczak, A. M. & Bakken, M. Behavioural evaluation of methods for assessing fear responses in weaned pigs. *Appl Anim. Behav. Sci.* **69**, 227–240 (2000).
34. Baroja-Mazo, A. et al. The NLRP3 inflammasome is released as a particulate danger signal that amplifies the inflammatory response. *Nat. Immunol.* **15**, 738–748 (2014).
35. Chivero, E. T., Guo, M. L. & Periyasamy, P. HIV-1 Tat primes and activates microglial NLRP3 inflammasome-mediated neuroinflammation. *J. Neurosci.* **37**, 3599–3609 (2017).
36. Ichinohe, T., Pang, I. K. & Iwasaki, A. Influenza virus activates inflammasomes via its intracellular M2 ion channel. *Nat. Immunol.* **11**, 404–410 (2010).
37. Hafner-Bratkovic, I., Bencina, M., Fitzgerald, K. A., Golenbock, D. & Jerala, R. NLRP3 inflammasome activation in macrophage cell lines by prion protein fibrils as the source of IL-1beta and neuronal toxicity. *Cell Mol. Life Sci.* **69**, 4215–4228 (2012).
38. Negash, A. A. et al. IL-1beta production through the NLRP3 inflammasome by hepatic macrophages links hepatitis C virus infection with liver inflammation and disease. *PLoS Pathog.* **9**, e1003330 (2013).
39. Chandy, K. G. & Norton, R. S. Peptide blockers of Kv1.3 channels in T cells as therapeutics for autoimmune disease. *Curr. Opin. Chem. Biol.* **38**, 97–107 (2017).
40. Chiang, E. Y. et al. Potassium channels Kv1.3 and KCa3.1 cooperatively and compensatorily regulate antigen-specific memory T cell functions. *Nat. Commun.* **8**, 14644 (2017).
41. Maezawa, I. et al. Kv1.3 inhibition as a potential microglia-targeted therapy for Alzheimer's disease: preclinical proof of concept. *Brain* **141**, 596–612 (2018).
42. Upadhyay, S. K. et al. Selective Kv1.3 channel blocker as therapeutic for obesity and insulin resistance. *Proc. Natl Acad. Sci. USA* **110**, E2239–E2248 (2013).
43. Di Lucente, J., Nguyen, H. M. & Wulff, H. The voltage-gated potassium channel Kv1.3 is required for microglial pro-inflammatory activation in vivo. *Glia* **66**, 1881–1895 (2018).
44. Liu, X. & Quan, N. Microglia and CNS Interleukin-1: Beyond Immunological Concepts. *Front Neurol.* **9**, 8 (2018).
45. Corasaniti, M. T. et al. 17beta-estradiol reduces neuronal apoptosis induced by HIV-1 gp120 in the neocortex of rat. *Neurotoxicology* **26**, 893–903 (2005).
46. Zhou, C. et al. Interleukin-1beta downregulates the L-type Ca2 + channel activity by depressing the expression of channel protein in cortical neurons. *J. Cell Physiol.* **206**, 799–806 (2006).
47. Yu, J. et al. IL-1beta stimulates brain-derived neurotrophic factor production in eutopic endometriosis stromal cell cultures: a model for cytokine regulation of neuroangiogenesis. *Am. J. Pathol.* **188**, 2281–2292 (2018).
48. Corasaniti, M. T. et al. Evidence that increases of mitochondrial immunoreactive IL-1beta by HIV-1gp120 implicate in situ cleavage of pro-IL-1beta in the neocortex of rat. *J. Neurochem.* **78**, 611–618 (2001).
49. Russo, R. et al. Evidence implicating matrix metalloproteinases in the mechanism underlying accumulation of IL-1beta and neuronal apoptosis in the neocortex of HIV/gp120-exposed rats. *Int Rev. Neurobiol.* **82**, 407–421 (2007).
50. Lipton, S. A. & Gendelman, H. E. Seminars in medicine of the Beth Israel Hospital, Boston. Dementia associated with the acquired immunodeficiency syndrome. *N. Engl. J. Med.* **332**, 934–940 (1995).
51. Block, M. L., Zecca, L. & Hong, J. S. Microglia-mediated neurotoxicity: uncovering the molecular mechanisms. *Nat. Rev. Neurosci.* **8**, 57–69 (2007).
52. Valderrama, J. A., Riestra, A. M., Gao, N. J. & LaRock, C. N. Group A streptococcal M protein activates the NLRP3 inflammasome. *Nat. Microbiol.* **2**, 1425–1434 (2017).
53. Ashraf, T. et al. Role of anti-inflammatory compounds in human immunodeficiency virus-1 glycoprotein120-mediated brain inflammation. *J. Neuroinflamm.* **11**, 91 (2014).
54. Bachis, A., Cruz, M. I. & Mocchetti, I. M-tropic HIV envelope protein gp120 exhibits a different neuropathological profile than T-tropic gp120 in rat striatum. *Eur. J. Neurosci.* **32**, 570–578 (2010).
55. Wang, Y., Liao, J., Tang, S. J., Shu, J. & Zhang, W. HIV-1gp120 upregulates brain-derived neurotrophic factor (BDNF) expression in BV2 cells via the Wnt/β-catenin signaling pathway. *J. Mol. Neurosci.* **62**, 199–208 (2017).
56. Luo, W., Fang, W., Li, S. & Yao, K. Aberrant expression of nuclear vimentin and related epithelial–mesenchymal transition markers in nasopharyngeal carcinoma. *Int. J. Cancer* **131**, 1863–1873 (2012).
57. Huang, S.-H. et al. Vimentin, a Novel NF-κB regulator, is required for meningitic Escherichia coli K1-induced pathogen invasion and PMN transmigration across the blood-brain barrier. *PloS One* **11**, e0162641 (2016).
58. Dos Santos, G. et al. Vimentin regulates activation of the NLRP3 inflammasome. *Nat. Commun.* **6**, 6574 (2015).
59. Hol, E. M. & Pekny, M. Glial fibrillary acidic protein (GFAP) and the astrocyte intermediate filament system in diseases of the central nervous system. *Curr. Opin. Cell Biol.* **32**, 121–130 (2015).
60. El-Barbary, A. M., Kassem, E. M., El-Sergany, M. A., SALWA, A. & Eltomey, M. A. Association of anti-modified citrullinated vimentin with subclinical atherosclerosis in early rheumatoid arthritis compared with anti-cyclic citrullinated peptide. *J. Rheumatol.* **38**, 828–834 (2011).
61. Thomas, E. K. et al. Anti-idiotypic antibody to the V3 domain of gp120 binds to vimentin: a possible role of intermediate filaments in the early steps of HIV-1 infection cycle. *Viral Immunol.* **9**, 73–87 (1996).
62. Noda, H., Takeuchi, H., Mizuno, T. & Suzumura, A. Fingolimod phosphate promotes the neuroprotective effects of microglia. *J. Neuroimmunol.* **256**, 13–18 (2013).
63. Meeker, R. B., Poulton, W., Clary, G., Schriver, M. & Longo, F. M. Novel p75 neurotrophin receptor ligand stabilizes neuronal calcium, preserves mitochondrial movement and protects against HIV associated neuropathogenesis. *Exp. Neurol.* **275**, 182–198 (2016).
64. Dreyer, E. B., Kaiser, P. K., Offermann, J. T. & Lipton, S. A. HIV-1 coat protein neurotoxicity prevented by calcium channel antagonists. *Science* **248**, 364–367 (1990).
65. Ashkenazi, A. et al. Polyglutamine tracts regulate beclin 1-dependent autophagy. *Nature* **545**, 108–111 (2017).
66. Moss, P. J. et al. Macrophage–sensory neuronal interaction in HIV-1 gp120-induced neurotoxicity. *Br. J. Anaesth.* **114**, 499–508 (2014).
67. Keswani, S. C. et al. Schwann cell chemokine receptors mediate HIV-1 gp120 toxicity to sensory neurons. *Ann. Neurol.* **54**, 287–296 (2003).
68. Higgins, S., Lee, J. S., Ha, L. & Lim, J. Y. Inducing neurite outgrowth by mechanical cell stretch. *BioResearch Open Access* **2**, 212–216 (2013).